Hamaker constants of inorganic materials

Lennart Bergström

Institute for Surface Chemistry, P.O. Box 5607, S-114 86 Stockholm, Sweden

Abstract

Calculations of Hamaker constants using Lifshitz theory require the availability of accurate dielectric data, especially in the ultraviolet spectral region, and the use of a convenient and appropriate mathematical representation. In this review, a multiple oscillator model — the so-called Ninham–Parsegian (N–P) representation — has been used and spectral parameters for 31 different inorganic materials (including diamond) have been generated from critically evaluated optical data or collected from the literature. For most materials, a two-oscillator model (one UV and one IR term) was used but more detailed representations were included when available. The spectral parameters presented here can be combined with previous data, mainly focused on hydrocarbon and organic systems, to yield an extensive spectral data base for both solids and liquids enabling Lifshitz calculations of Hamaker constants for many materials combinations.

Non-retarded Hamaker constants for symmetric material combinations across vacuum (A_{1v1}) and water (A_{1w1}) have been calculated for the different materials; these calculations were performed using the full Lifshitz theory. Asymmetric combinations, A_{1v3} and A_{1w3}, against four commonly used materials in atomic force microscopy studies: silica, amorphous silicon nitride, sapphire, and muscovite mica, have also been covered. The use of a new dielectric representation for water resulted in significantly lower values of A_{1w1} compared to previous calculations. Analytical approximations to the full Lifshitz theory were evaluated and found to give surprisingly accurate results (the Tabor–Winterton approximation) for A_{1v1} when the IR contribution is of minor importance. An attempt to make the TW approximation more general by establishing some scaling relationship between n_0 and ω_{UV} was met with little success; only the UV spectral parameters of the covalent oxides, sulphides and nitrides may be fitted to a simple power law relation.

The Lifshitz calculations in this study were compared with an alternative method where a more detailed dielectric representation in the visible-ultraviolet spectral range was obtained through Kramers–Kronig (K–K) transformation of reflectivity data over a broad frequency range. Despite the difference in dielectric information, the two

methods generally yield non-retarded Hamaker constants which do not differ signifi-
cantly. This is not true for all materials, e.g. water, where a more detailed representation
using either an N–P representation with several oscillators or the K–K representation
must be used. It was shown that the omission of the static and low frequency contribution
in the latter method may result in a significant underestimation of the value for A_{1w1}
when the dispersive contribution becomes very small.

Keywords: Hamaker constant, van der Waals interaction, inorganic materials, interpar-
ticle forces, AFM

Contents

I. Introduction

The surface forces between two bodies in close proximity play an
important role in many scientific and technical areas, e.g. adhesion,
wetting, adsorption, colloidal phase equilibrium, flocculation rates, rheologi-
cal properties and other colloid and interface phenomena [1,2]. In phenom-
ena involving inorganic materials, examples include the important role of
interparticle forces in determining the rheological behaviour of the ceramic
suspensions in the powder preparation and consolidation step [2–4], and

the suggestion that a surface force balance controls the thickness of thin intergranular glass films in polycrystalline ceramics [5].

Among the many contributions to the interaction between surfaces, e.g. double layer, structural, steric, depletion, hydration and hydrophobic forces, there is one type of interaction which is always present, the van der Waals interaction. This ubiquitous interaction may be of varying importance depending on the system. The Hamaker constant represents a conventional and convenient way of assessing the magnitude of this interaction. Recent work has shown that many inorganic systems are characterised by relatively high Hamaker constants [6,7], hence making this interaction of significant importance. It is obvious that accurate estimations of the Hamaker constants is necessary for a quantitative understanding of the effect of interparticle forces on various phenomena.

The van der Waals force has an electrodynamic origin as it arises from the interactions between atomic or molecular oscillating or rotating electrical dipoles within the interacting media. There are three types of interactions which contribute to the van der Waals force:

(i) The Keesom force which is the interaction between two permanent dipoles.

(ii) The Debye force which is the interaction between one permanent dipole and one induced dipole.

(iii) The London or dispersion force which is the interaction between two induced dipoles.

Between molecules, each of these contributions has an interaction free energy which varies with the inverse sixth power of the distance at small and intermediate distances of separation (from 1–2 Å to several nm).

Hamaker [8] calculated the distance dependence of the free energy of macroscopic bodies by performing a pair-wise summation over all the atoms in the bodies. For example, the van der Waals interaction free energy, V_{vdW}, per unit area, between semi-infinite parallel plates at separation, L, can be expressed as

$$V_{vdW} = -\frac{A}{12\pi L^2} \tag{1}$$

where A is the Hamaker constant. As seen in Eq. (1), there is a direct proportionality between the magnitude of the van der Waals interaction and the Hamaker constant. The Hamaker constant is a materials constant that depends on the properties of the two materials and the intervening media. The distance dependence of the van der Waals energy depends essentially on the geometry of the two interacting bodies

being proportional to L^{-2} for parallel plates and scale to L^{-1} for two spherical particles at short separation distances where retardation can be ignored.

In the original treatment, also called the microscopic approach, the Hamaker constant was calculated from the polarizabilities and number densities of the atoms in the two interacting bodies [8]. Lifshitz presented an alternative, more rigorous approach where each body is treated as a continuum with certain dielectric properties [9]. This approach automatically incorporates many-body effects which is neglected in the microscopic approach. In the Lifshitz treatment, the van der Waals interaction is the result of fluctuations in the electromagnetic field between two macroscopic bodies, modified by the separating media, where the interaction can be referred to the standing waves which only occur at certain frequencies. Hence, the van der Waals interaction, and thus the associated Hamaker constants, can be estimated from a knowledge of the frequency dependent dielectric properties of the interacting materials together with the intervening medium, and the geometry of the bodies. The accuracy of the estimated Hamaker constants are directly related to the precision and accuracy of the dielectric spectra and the mathematical representation of this data.

The main focus of this review is to provide a collection of dielectric representations for a range of inorganic materials presented in a condensed but appropriate manner, suitable for calculations of accurate Hamaker constants. The dielectric representation follows the form presented by Hough and White [10] in their collection of spectral parameters and Hamaker constants for a number of materials, focusing mainly on liquids and organic solids. Since their work was published, collections of accurate dielectric data for many inorganic materials have become easily available [11,12] which makes the determination of the necessary spectral parameters an easy task. The two handbooks of Optical Constants of Solids I and II [11,12] will constitute the main source of dielectric spectral information but previously published data will also be included.

In the next, theoretical section, the basis of the dielectric response representation and an outline of the Lifshitz theory for van der Waals forces together with a description of simplifying assumptions made to facilitate calculations will be described. It should be noted that no theoretical advances are being presented here; the theoretical section completely relies on previously published material and merely forms a basis for the estimations of spectral parameters and calculations of

Hamaker constants. This is followed by a presentation of dielectric data and discussion how the spectral parameters in the ultraviolet (UV) and the infrared (IR) frequency range can be determined. The spectral parameters for 31 different inorganic materials (including diamond) are either taken directly from the literature or estimated from data on the static dielectric constant, $\varepsilon(0)$, the frequency dependence of the refractive index, $n(\omega)$, in the UV frequency range, and the frequency of the strongest IR-absorption band.

Non-retarded Hamaker constants for the inorganic materials across vacuum and water was calculated using the full Lifshitz theory. In addition, Hamaker constants for systems important in atomic force microscopy (AFM) studies have also been calculated. A recently published improved spectral parametric representation of water [13] has been used for these calculations which resulted in some significant changes compared to previous estimates. The full Lifshitz calculations have been compared with various analytical simplifications and a surprisingly good agreement was found for the Hamaker constants with vacuum as the intervening medium. The importance of the IR range for the calculation of Hamaker constants was evaluated. In the final section, the Hamaker constants obtained in this study were compared with calculations based on an alternative dielectric representation using Kramers–Kronig relations.

II. Theory

IIA. Dielectric response

The dielectric properties of a material are commonly represented by the frequency dependent dielectric response function, $\varepsilon(\omega)$

$$\varepsilon(\omega) = \varepsilon'(\omega) + i\varepsilon''(\omega) \tag{2}$$

which is a complex function where $\varepsilon'(\omega)$ is the real part, and $\varepsilon''(\omega)$ the imaginary part. This function is intimately related to the transmission ($\varepsilon'(\omega)$) and absorption ($\varepsilon''(\omega)$) of the applied electromagnetic radiation. In frequency regions where $\varepsilon''(\omega)$ is zero, the material is transparent and the real part of the dielectric response is directly related to the refractive index, $n(\omega)$ through

$$\varepsilon(\omega) = \varepsilon'(\omega) = n^2(\omega) \tag{3}$$

For a static applied field ($\omega = 0$), non-conductor materials are characterised by $\varepsilon''(\omega) \approx 0$, hence $\varepsilon'(0) = \varepsilon(0)$ which is the static dielectric constant.

As a completely equivalent alternative to the dielectric response function, $\varepsilon(\omega)$, can the complex refractive index , $N(\omega)$, be used

$$N(\omega) = n(\omega) - ik(\omega) \tag{4}$$

which might be more familiar to some readers. The real part, $n(\omega)$, represents the refractive index and $k(\omega)$ is the extinction coefficient. Remembering the transmission and absorption dependence of the complex dielectric function, the mathematical connection between $\varepsilon(\omega)$ and $N(\omega)$ can be expressed as:

$$\varepsilon(\omega) = N^2(\omega) \tag{5}$$

$$N^2(\omega) = (n(\omega) - ik(\omega))^2 \tag{6}$$

$$\varepsilon'(\omega) = n^2(\omega) - k^2(\omega) \tag{7}$$

$$\varepsilon''(\omega) = 2n(\omega)k(\omega) \tag{8}$$

Dielectric data can be obtained with a number of methods including capacitance bridge, optical reflectance and ellipsometric techniques, and electron loss spectroscopy. Most of these techniques yield only one of the components of the complex dielectric response function which often necessitate the transformation from the real to the imaginary component or *vice versa*. Such a transformation can be performed using the Kramers–Kronig (K–K) relations, one of them defined as

$$\varepsilon'(\omega) = 1 + \frac{2}{\pi} \int\limits_0^\infty \frac{x\varepsilon''(\omega)}{x^2 - \omega^2}\, dx \tag{9}$$

where x represents real values of the frequency. The K–K relation in Eq. (9) shows that if $\varepsilon''(\omega)$ (i.e. the absorption spectrum) is known in the entire frequency range, $0 \le \omega < \infty$, then $\varepsilon'(\omega)$ can be fully defined. Similar K–K relations can be defined for other dielectric properties such as the frequency dependent interband transition strength [7].

Ninham and Parsegian [14,15] showed that by constructing an imaginary dielectric response function, $\varepsilon(i\xi_m)$, a much simpler dielectric representation could be used for the purpose of calculating Hamaker constants. Hough and White [10] have given a thorough analysis of this representation. The reason for using this imaginary representation is

completely mathematical, the imaginary part of the frequency has no physical significance that refers to the materials behaviour. The complex imaginary function decreases monotonically from ε_0 when $\xi = 0$, and goes to 1 as ξ approaches infinity. The final form of the Lifshitz expression for calculation of Hamaker constants (see next section) shows that imaginary dielectric function only has to be evaluated at discrete, equally spaced imaginary frequencies, $i\xi_m$, with

$$\xi_m = m(4\pi^2 k_B T/h) \tag{10}$$

where h is Planck's constant, k_B represents Boltzmann's constant, m is an integer; $m = 0,1,2,3,4..$, and T is the temperature in Kelvin. The imaginary dielectric response function, $\varepsilon(i\xi_m)$, can be obtained from $\varepsilon''(\omega)$ using another Kramers–Kronig relation [10]:

$$\varepsilon(i\xi) = 1 + \frac{2}{\pi} \int_0^\infty \frac{x\varepsilon''(x)}{x^2 + \xi^2} \, dx \tag{11}$$

The K–K relation in Eq. (10) has been used in several studies to construct the necessary $\varepsilon(i\xi_m)$ function [7,16,17] for estimations of Hamaker constants. However, since the K–K relation is formally correct only when $\varepsilon''(\omega)$ is known in the entire frequency range, $0 \le \omega < \infty$, this procedure is prone to numerical error since approximations for parts of the absorption spectrum invariably has to be used due to lack of spectral information.

With limited dielectric data available, the function $\varepsilon(i\xi_m)$ is usually represented by a model based on a damped oscillator. The so-called Ninham–Parsegian (N–P) representation of $\varepsilon(i\xi)$ can be given as [14,15, 18,19]

$$\varepsilon(i\xi_m) = 1 + \frac{B}{1 + \xi\tau} + \sum_{j=1}^N \frac{C_j}{1 + (\xi/\omega_j)^2 + g_j\xi/\omega_j^2} \tag{12}$$

where the first term after unity represents the contribution from the orientation of permanent dipoles (present in polar liquids like water), and the final summation relates to the absorption peaks in the infrared and ultraviolet range. B and g_j are related to the oscillator strength in the microwave range and damping coefficient of the oscillator, respectively, and C_j is represented by

$$C_j = \frac{2}{\pi} \frac{f_j}{\omega_j} \tag{13}$$

where f_j is the oscillator strength and ω_j is the relaxation frequency (in the unit rad/s) of the absorption band. The N–P representation simplifies the construction of the required function $\varepsilon(i\xi_m)$ since the frequencies and relative strengths of the peaks in the absorption spectrum can be used. With a well-characterised absorption spectrum over a relatively wide frequency range, many spectral parameters can be defined. Water is such a material and spectral parameters in the ultraviolet, infrared as well as the microwave range have been determined [13,20]. Roth and Lenhoff [13] have recently published an improved UV representation of water based on previously published reflectivity data [21]. Figure 1 shows that the real and imaginary dielectric data in the important frequency range can be closely fitted by using the summation in Eq. (12) and six UV terms including band widths. The full spectral representation of water including one microwave term and five infrared terms from Parsegian [20] and the six UV terms from Roth and Lenhoff [13] are collected in Table 1.

The accuracy of Hamaker constants calculated from Lifshitz theory relies on the quality of the experimental dielectric data and the accuracy of the spectral representation. With dielectric data over a wide frequency range, the two alternative methods: K–K transformation using Eq. (11), or the N–P representation, Eq. (12), should yield a similar result. If the dielectric data is limited, both approaches may result in inaccurate representations. The K–K transformation is sensitive to the

Table 1

Spectral parameters* for water**

C_{UV}	$\omega_{UV} \times 10^{16}$ (rad/s)	$g_{UV} \times 10^{15}$ (rad/s)	C_{IR}	$\omega_{IR} \times 10^{14}$ (rad/s)	$g_{IR} \times 10^{13}$ (rad/s)
0.0484	1.25	0.957	1.46	0.314	2.29
0.0387	1.52	1.28	0.737	1.05	5.78
0.0923	1.73	3.11	0.152	1.40	4.22
0.344	2.07	5.92	0.0136	3.06	3.81
0.360	2.70	11.1	0.0751	6.46	8.54
0.0383	3.83	8.11			

$B = 76.8$ and $1/\tau_{MW} = 1.08 \times 10^{11}$ rad/s.

* C_{IR} and C_{UV} are the absorption strengths, and ω_{IR} and ω_{UV} represent the characteristic absorption frequencies in the IR and UV range, respectively. The damping terms are denoted by g_{IR} and g_{UV}.

** UV representation from Roth and Lenhoff [13], and IR and microwave representation from Parsegian [20].

(a)
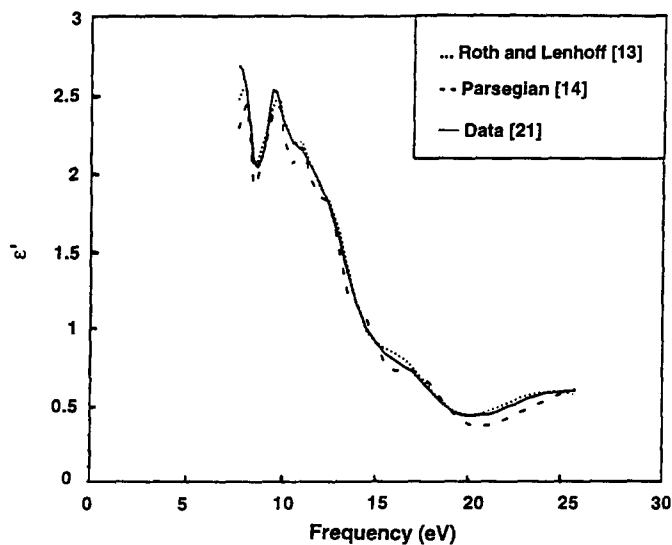
(b)
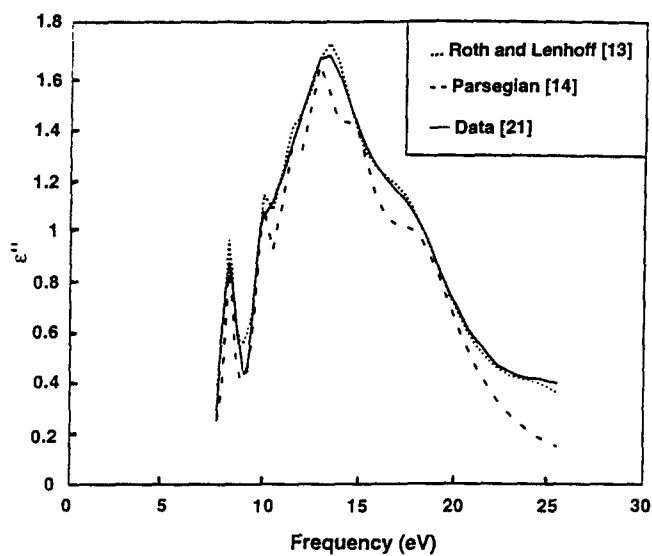
Fig. 1. Comparison of experimental dielectric data (solid line) for water of the real (a) and imaginary (b) component [21], and two different mathematical representations (broken lines) from Parsegian [14] and Roth and Lenhoff [13]. Each representation uses six oscillators including band widths. From Roth and Lenhoff [13].

approximations outside the available spectral data, and the N–P representation, using a limited number of oscillators, may be of poor quality for materials with complicated spectral features.

However, there is some evidence that many materials with "simpler" spectral features can be reasonably well described by less complicated N–P representations [10]. At room temperature, ξ_m are sampled at integral multiples of 2.4×10^{14} rad/s which corresponds to one static term, only a few terms in the infrared and many in the visible–ultraviolet region. Hence, since the dielectric response in the visible–UV range completely dominates the van der Waals interaction for most systems, it is of outmost importance to have access to accurate spectral data in this frequency range. In this study, $\varepsilon(i\xi_m)$ for most of the inorganic materials will be represented by one UV and one IR relaxation

$$\varepsilon(i\xi_m) = 1 + \frac{C_{IR}}{1 + (\xi / \omega_{IR})^2} + \frac{C_{UV}}{1 + (\xi / \omega_{UV})^2} \tag{14}$$

where each material is characterised by four parameters; C_{IR} and C_{UV} are the absorption strengths in the IR and UV range, respectively, and ω_{IR} and ω_{UV} represent the characteristic absorption frequencies in the IR and UV range, respectively. The damping terms are omitted. In some cases when a more detailed representation has already been presented, this data will be included. The limitations and accuracy of this dielectric representation will be discussed in more detail later.

IIB. Calculation of non-retarded Hamaker constants

The interaction free energy per unit area, E_{132}, between two half-spaces of material 1 and material 2 interacting over media 3, can in the non-retarded approximation (small separation distance, L) be written as [9,10,18]

$$E_{132} = \frac{k_B T}{2\pi} \sum_{m=0}^{\infty}{}' \int_0^{\infty} y dy \ln(1 - \Delta_{13}\Delta_{23} e^{-2yL}) \tag{15}$$

with the differences in dielectric response, Δ_{kl}, defined as

$$\Delta_{kl} = \frac{\varepsilon_k(i\xi_m) - \varepsilon_l(i\xi_m)}{\varepsilon_k(i\xi_m) + \varepsilon_l(i\xi_m)} \tag{16}$$

where $\varepsilon_k(i\xi_m)$ and $\varepsilon_l(i\xi_m)$ are the dielectric response function of material k and l, respectively, evaluated at the imaginary frequency, $i\xi_m$ according to Eq. (10). The prime on the first summation in Eq. (15) indicates that the $m = 0$ term (the static contribution) is given half weight. By a change of variables ($x = 2yL$), it is possible to define E_{132} according to Eq. (1),

$$E_{132} = -\frac{A_{132}}{12\pi L^2} \tag{17}$$

thus identifying the non-retarded Hamaker constant A_{132} which is given as

$$A_{132} = \frac{3k_B T}{2} \sum_{m=0}^{\infty}{}' \int_0^{\infty} dx\, x \ln(1 - \Delta_{13}\Delta_{23}\, e^{-x}) \tag{18}$$

This integral can be performed analytically to yield

$$A_{132} = \frac{3k_B T}{2} \sum_{m=0}^{\infty}{}' \sum_{s=1}^{\infty} \frac{(\Delta_{13}\Delta_{23})^s}{s^3} \tag{19}$$

A detailed account of how this double summation equation (Eq. (19)) is derived directly from the original expression given by Lifshitz [9] can be found in previous work [18]. The frequency sum can be replaced by an integral to yield

$$A_{132} = \frac{3h}{8\pi^2} \int_0^{\infty} d\xi \sum_{s=1}^{\infty} \frac{(\Delta_{13}\Delta_{23})^s}{s^3} \tag{20}$$

which is correct only in the limit, $T \to 0$, where the distance between the sampled frequencies (Eq. (10)) tend to zero [9,18]. This transformation is equivalent to omitting the static term ($m = 0$, $\xi = 0$) in the frequency summation (Eq. (19)). The temperature independent dispersive part of the non-retarded Hamaker constant, represented by the summation $m > 1$, however, is not affected by the transformation. Hence, when the static contribution to the non-retarded Hamaker constant is negligible, the error of using Eq. (20) will be minor. However, when water or another material characterised by a high static dielectric constant is one part of the system, the static contribution may be significant thus restricting the use of the integral equation (Eq. (20)).

This will be illustrated in more depth later. Also, at elevated temperatures, the static contribution to the Hamaker constant may be large.

Simplified approximations for less accurate estimations of non-retarded Hamaker constants have been derived for a number of cases by only retaining a single UV relaxation to represent the dielectric response of each material. These simplifications have been motivated by the pivotal role of the ultraviolet relaxations on the magnitude of the dispersive interactions. With such a simple dielectric representation, each material is fully described by three parameters, $\varepsilon(0)$, the characteristic frequency in the ultraviolet, ω_{UV}, and the low-frequency limit of the refractive index in the visible–UV range, n_0 (since $C_{UV} = n_{vis}^2 - 1$).

For example, the non-retarded Hamaker constant for two identical materials 1, interacting across a medium 3 was calculated by using Eq. (19), neglecting all summation terms $s > 1$, converting the summation over n to an integral for $m > 1$, and finally setting $\omega_1 \approx \omega_3 \approx \omega$. This results in [1]

$$A_{131} = \frac{3kT}{4}\left(\frac{\varepsilon_1(0) - \varepsilon_3(0)}{\varepsilon_1(0) + \varepsilon_3(0)}\right)^2 + \frac{3h\omega}{32\pi\sqrt{2}}\frac{(n_1^2 - n_3^2)^2}{(n_1^2 + n_3^2)^{3/2}} \tag{21}$$

where the first term on the right hand side represents the static contribution and the second term represents the dispersive contribution and n_1 and n_3 is the refractive index in the visible of the material and medium, respectively. If the medium is vacuum and the static contribution is ignored, Eq. (21) reduces to the so called Tabor–Winterton (TW) representation [22]. A more complicated expression for the dispersive contribution is obtained if the interacting material and the medium are allowed to have different absorption frequencies $\omega_1 \neq \omega_3$ [23].

$$A_{disp,131} = 3h\frac{\sqrt{\omega_1\omega_3}}{128\pi\bar{\varepsilon}^{7/4}}\frac{(X^2\bar{\varepsilon} + 2X\Delta\varepsilon\,\bar{\varepsilon}^{1/2} + \Delta\varepsilon^2(3 + 2Y))}{\left[(Y - \sqrt{Y^2 - 1})^{1/2} + (Y + \sqrt{Y^2 - 1})^{1/2}\right]^3} \tag{22}$$

where

$$\bar{\varepsilon} = 0.5(n_1^2 + n_3^2)$$

$$\Delta\varepsilon = n_1^2 - n_3^2$$

$$X = \frac{\omega_1}{\omega_3}(n_1^2 - 1) - \frac{\omega_3}{\omega_1}(n_3^2 - 1)$$

$$Y = \frac{1}{4\bar{\varepsilon}^{1/2}} \left[\frac{\omega_1}{\omega_3} (n_1^2 + 1) + \frac{\omega_3}{\omega_1} (n_3^2 + 1) \right]$$

It may be shown that Eq. (22) will be identical to the dispersive part of Eq. (21) if ω_1 and ω_3 are replaced with ω. These approximations of the non-retarded Hamaker constant and others representing dissimilar materials across a dielectric and interactions between coated materials have been presented in a condensed form by Prieve and Russel [19]. In this study, the appropriateness of the different approximations for inorganic materials will be evaluated and the importance of the IR-range and the static contribution to the magnitude of the Hamaker constant will be evaluated. For the full Lifshitz calculations using Eq. (19), a summation over $s = 1$ to 4 and the first 3000 terms of m where employed.

III. Dielectric representation

IIIA. Dielectric data of materials

The dielectric response can be directly referred to the electronic and vibrational states of a material. In the infrared region, lattice vibrations dominate while in the ultraviolet–visible frequency range, electronic or interband transitions dominate for a non-conducting solid. There is a wealth of data on the frequency dependence of the optical properties of solid inorganic materials available in the literature. Many inorganic materials have been critically summarised in the two Handbooks of Optical Constants of Solids [11,12] which constitute an excellent source of data for the present task of elucidating spectral parameters for inorganic materials.

Some recently published optical data on ceramic materials [6] illustrate the typical features of the optical characteristics in the important UV–visible range. Figure 2 shows a plot of the refractive index, $n(\omega)$, and extinction coefficient, $k(\omega)$ (ZnO only), as a function of photon energy for the polycrystalline materials: 6H-SiC, tetragonal ZrO_2, α-Al_2O_3, and ZnO based on spectroscopic ellipsometry measurements. Three of these materials: SiC, ZrO_2 and Al_2O_3, display the normal dispersive behaviour of a transparent material; the refractive index increases with an increase in photon energy (frequency). This is related to a low photon absorption with the extinction coefficient, $k(\omega)$, close to zero and always below 0.1 (not shown). ZnO on the other hand, shows a distinct peak in the refractive index and a sharp increase in the extinction coefficient at

(a)

(b)
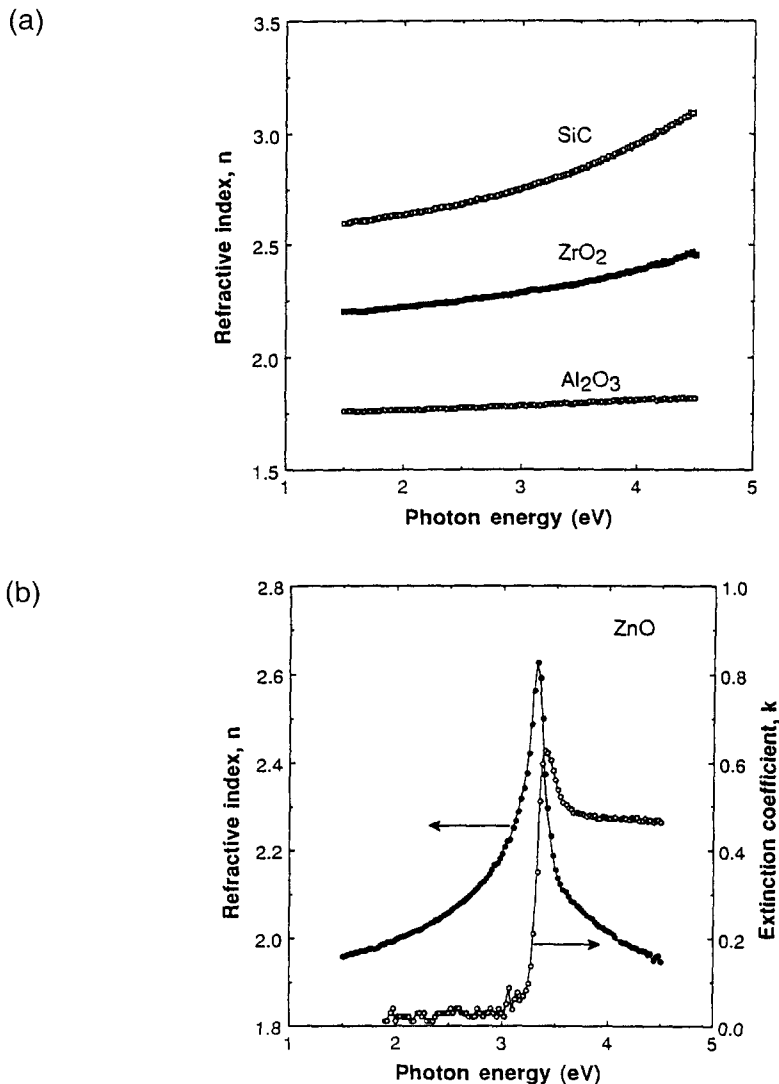
Fig. 2. Optical characteristics versus photon energy from ellipsometry measurements for (a) 6H-SiC, tetragonal, partially stabilized ZrO_2, and α-Al_2O_3; and (b) ZnO. Taken from Ref. [6].

a critical photon energy. At photon energies below 3.2 eV, the extinction coefficient is close to zero ($k < 0.05$). However, above 3.3 eV, k suddenly increases to $k > 0.5$. Hence the material ceases to be transparent in the high photon energy range. This transition is associated with an electronic excitation since ZnO is a semiconductor with a bandgap at 3.3 eV [24].

For the simplified spectral representation used in this study, optical data over a relatively narrow frequency range (as shown in Fig. 2) suffices for the elucidation of the UV term. However, if a more detailed spectral representation of the ultraviolet spectral region is to be constructed, dielectric data over a wider frequency range is needed, as illustrated for water in Fig. 1.

Anisotropic materials can display different dielectric responses in different crystal orientations. This can be represented by a dielectric response function in tensorial form where the number of independent components depends on the crystal symmetry. Cubic systems only have one component, i.e. display no anisometry, while tetragonal, hexagonal and trigonal systems have two components, resulting in optical birefringence. More complicated crystal forms such as orthorhombic, monoclinic and triclinic systems display a higher number of components. In a birefringent material, the following nomenclature is often used:

n_0, $n_\perp$ = ordinary ray, E perpendicular to the optical axis
n_{eo}, $n_{//}$ = extraordinary ray, E parallel to the optical axis

where E denotes the electric field. The separate components can only be determined for single crystals while polycrystalline materials yields an average due to the random orientation of the grains.

IIIB. Determination of spectral parameters

In the simplified representation of the $\varepsilon(i\xi_m)$ function used in this study, the ultraviolet frequency region is represented by only one oscillator which can be written as

$$\varepsilon(i\xi_m) = 1 + \frac{C_{UV}}{1 + (\xi/\omega_{UV})^2} \tag{23}$$

valid at frequencies below the band gap and much above the infrared absorption band. For materials that do not absorb in the visible and UV range, the dielectric spectrum is simplified according to Eq. (3). Hough and White [10] utilised a simple graphic method of obtaining ω_{UV} and C_{uv} from the frequency dependence of the refractive index, $n(\omega)$; the so-called "Cauchy equation"

$$n^2(\omega) - 1 = (n^2(\omega) - 1)\frac{\omega^2}{\omega_{UV}^2} + C_{UV} \tag{24}$$

which should result in a linear plot of $[(n^2(\omega) - 1)]$ versus $[(n^2(\omega) - 1)\,\omega^2]$.

Table 2

Spectral parameters* for various inorganic materials

Material**	Crystal structure	$\epsilon(0)$	C_{UV}	n_0	ω_{UV} (10^{16} rad/s)	C_{IR}	ω_{IR} (10^{14} rad/s)
$\alpha\text{-Al}_2\text{O}_3$	hexagonal	10.1	2.072	1.753	2.00	7.03	1
BaTiO_3 o	tetragonal	3600	4.218	2.284	0.841	3595	0.7–1.0
eo		150	4.064	2.25	0.896	145	0.7–1.0
BaTiO_3 (average)	tetragonal	2400	4.164	2.272	0.857	2394	0.7–1.0
BeO o	hexagonal	6.94	1.90	1.703	1.98	4.04	1.3
eo		7.95	1.951	1.718	2.37	4.70	1.4
BeO (average)	hexagonal	7.18	1.917	1.708	2.11	4.26	1.3
C (diamond IIa)	cubic	5.66	4.642	2.375	1.61	0.02	2.5
CaCO_3 o	trigonal	8.0	1.683	1.638	1.660	5.3	–
(calcite) eo		8.5	1.182	1.477	2.134	6.3	–
CaCO_3 (average)	trigonal	8.2	1.516	1.586	1.897	5.7	2.691
CaF_2	cubic	6.7	1.036	1.427	2.366	4.66	0.55
CdS	hexagonal	9.97	4.114	2.261	0.692	4.86	0.46
CsI	cubic	6.54	2.000	1.732	1.11	3.54	0.12
$\text{KAl}_2\text{Si}_3\text{AlO}_{10}(\text{OH})_2$	monoclinic	5.4	1.508	1.584	1.963	1.041	0.986
(muscovite mica)						0.451	1.559
						0.714	1.753
						0.686	1.866
KBr	cubic	4.8	1.344	1.531	1.32	2.46	0.21
KCl	cubic	4.4	1.170	1.473	1.58	2.23	0.27
LiF	cubic	9.06	0.924	1.387	2.53	7.14	0.58
MgAl_2O_4	cubic	8.3	1.887	1.699	1.87	5.41	1.0
MgF_2	tetragonal	5.47	0.8835	1.372	2.550	3.59	0.47

Material**	Crystal structure	$\varepsilon(0)$	C_{UV}	n_0	ω_{UV} $(10^{16}$ rad/s)	C_{IR}	ω_{IR} $(10^{14}$ rad/s)
MgO	cubic	9.8	1.946	1.716	1.71	6.85	1.0
NaCl	cubic	5.9	1.325	1.525	1.55	3.58	0.31
NaF	cubic	5.7	0.7417	1.32	2.28	3.96	0.46
PbS	cubic	169	15.04	4.005	0.167	153	0.14
6H-SiC	hexagonal	10.2	5.526	2.555	1.14	3.67	1.6
β-SiC	cubic	9.72	5.424	2.534	1.15	3.30	1.5
β-Si$_3$N$_4$	hexagonal	8.7	2.858	1.964	1.61	4.84	1.7
Si$_3$N$_4$	amorphous	7.4	2.953	1.988	1.448	1.08	0.90
						2.37	1.64
SiO$_2$ (quartz)	trigonal	4.29	1.359	1.536	2.032	1.93	2.093
SiO$_2$ (silica)	amorphous	3.82	1.098	1.448	2.034	0.829	0.867
						0.095	1.508
						0.798	2.026
SrTiO$_3$	cubic	311	4.152	2.27	0.863	306	0.4
TiO$_2$ (rutile) o	tetragonal	–	4.81		0.77	–	–
eo		–	5.62		0.686	–	–
TiO$_2$ (average)	tetragonal	114	5.07	2.464	0.735	108	0.7
Y$_2$O$_3$	hexagonal	11.8	2.574	1.891	1.35	8.23	0.7
ZnO	hexagonal	11.8	2.648	1.910	0.895	8.15	0.7
ZnS	cubic	8.35	4.081	2.254	0.939	3.27	0.54
ZnS	hexagonal	8.7	4.153	2.270	1.04	3.55	0.52
3Y-ZrO$_2$	tetragonal	18	3.743	2.178	1.34	13.26	1.88

* $\varepsilon(0)$ and n_0 are the static dielectric constant, and the limiting refractive index in the visible, respectively. Refer to Table 1 for explanation of the other spectral parameters.

** o and eo denote the ordinary and extraordinary ray, respectively. The average value was calculated using a weighing procedure.

Figures 3–6 show "Cauchy" plots based on optical data from the literature [11,12] for a number of inorganic materials. The data was selected from the frequency range where the materials display negligible extinction coefficients (below the band gap) and sufficiently above the IR absorption range. More details of the spectral data is given below for each of the materials. The slope and intercept of the straight lines were determined by least square regression, which yields C_{UV} and ω_{UV}. The UV–visible optical data for all the materials in this review can be well fitted to this type of single oscillator model. Materials where the optical data was too sparse or the Cauchy fit too poor, have not been included here. The values of the spectral parameters are collected in Table 2.

A simplified infrared representation was used since the infrared and microwave contribution to the $\varepsilon(i\xi_m)$ function usually is of minor importance. This is due to the sparse sampling which is related to the large spacing of the sampling frequencies, ξ_m is about 2.5×10^{14} rad/s at room temperature (see Eq. (10)). The spectral constant C_{IR} is given by

$$C_{IR} = \varepsilon(0) - C_{UV} - 1 \tag{25}$$

and the characteristic absorption frequency, ω_{IR}, will be defined as the frequency of the major absorption peak in the IR spectrum. The values of static dielectric constants for the different materials and the IR data were obtained from two major sources [12,25]. More details of the infrared data are given below for each material.

IV. Spectral parameters of materials

The values of both the IR and UV spectral parameters for the 31 inorganic materials (including diamond) are summarised in Table 2. The dielectric data or representation of each material is briefly described below. All the spectral data represents room-temperature values.

IVA. Amorphous materials

Two amorphous materials were included in Table 2: silicon nitride (Si_3N_4) and silica (SiO_2). Senden and Drummond [26] have published a thorough analysis of the spectral parameters of these materials in both the UV–visible and infrared spectral region, included in Table 2.

IVB. Cubic halides

All of the spectral parameters for the halides have been obtained from Cauchy plots (UV–visible spectral range), and infrared absorption peaks (IR spectral range) from the literature. Figure 3 shows that all of the cubic halides display a similar behaviour, well described by the single oscillator expression in the UV–visible range.

1. CaF_2

Bezuidenhout [27] has compiled the data for calcium fluoride which is a highly ionic compound having a cubic fluorite crystal structure. The data of Malitson [28] on the refractive index values in the ultraviolet–visible frequency range was used in the Cauchy plot (Fig. 3). The infrared absorption data from Kaiser et al. [29] was used to determine the frequency of the main absorption peak.
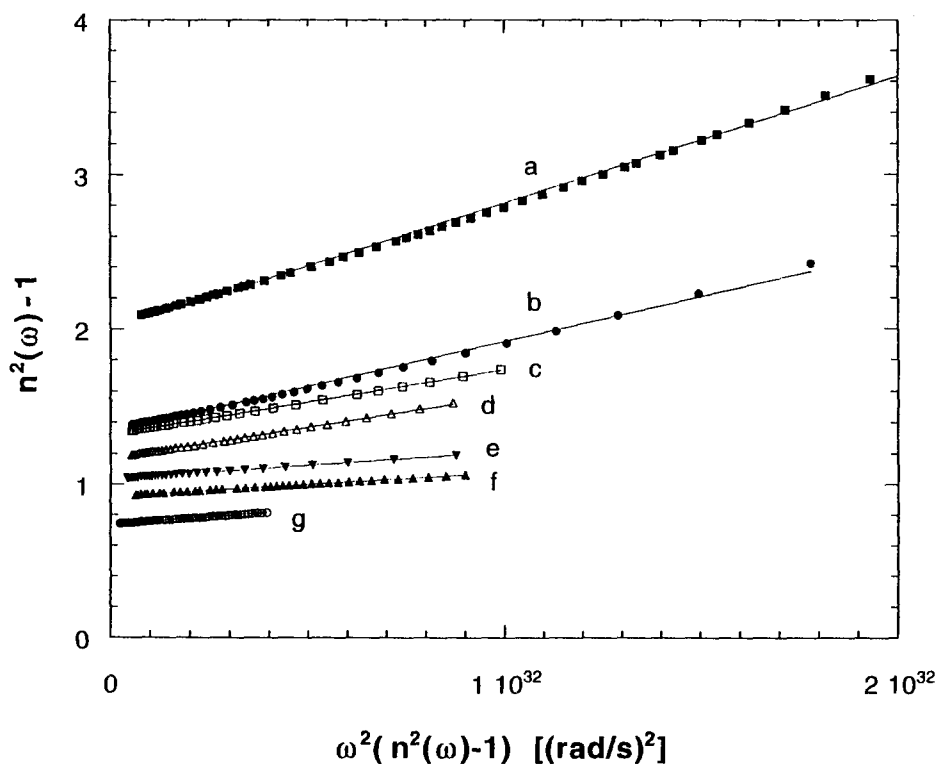
Fig. 3. Cauchy plots for the cubic ionic halide materials; (a) CsI, (b) KBr, (c) NaCl, (d) KCl, (e) CaF_2, (f) LiF, (g) NaF.

2. CsI

Cesium iodide which has a cubic CsCl structure does also display a very wide transmission band making it a common window material in infrared spectroscopy. Eldridge [30] has compiled the dielectric data and the ultraviolet–visible data used in the Cauchy plot (Fig. 3) were based on the tabulated values by Li [31]. The very low frequency of the infrared absorption peak was determined by Beairsto and Eldridge [32] using transmission measurements.

3. KBr

The spectral data of potassium bromide having a cubic rock salt crystal structure has been compiled by Palik [33]. The collection and analysis of refractive index data by Li [34] was used for the Cauchy plot in Fig. 3. Infrared data from Johnson and Bell [35] was used for absorption peak determination.

4. KCl

Palik [36] has also collected the spectral data of potassium chloride having a cubic rock salt crystal structure. The ultraviolet-visible data used in the Cauchy plot (Fig. 3) was based on refractive index data tabulated by Li [31]. The infrared absorption peak was identified with the transverse phonon frequency, also from Li [31].

5. LiF

Lithium fluoride also display the cubic rock salt crystal structure. The dielectric data has been compiled by Palik and Hunter [37], and the Cauchy plot in Fig. 3 is based on tabulated refractive index data by Li [38]. The identification of the main absorption peak in the infrared was based on the data by Kachare et al. [39].

6. NaCl

The refractive index data of sodium chloride used in the Cauchy plot in Fig. 3 was taken from Li [31] again, compiled by Eldridge and Palik [40]. The infrared data are from Eldridge and Staal [41].

7. NaF

The dielectric data of sodium fluoride, having a cubic rock salt crystal structure, was compiled by Ohlidal and Navratil [42]. The refractive index data in the ultraviolet–visible range was obtained from Harting [43], while the infrared data originates from Pai et al. [44].

IVC. Cubic covalent materials

The spectral parameters of two of the cubic, covalent materials, magnesium oxide (MgO) having a periclase structure and magnesium aluminate ($MgAl_2O_4$) having a spinel structure, were collected from a previous study using literature optical data [6].

1. C (diamond type IIa)

Although diamond (cubic carbon) cannot be classified as an inorganic solid, it was included in this review due to the general interest in this material. Diamond is classified into four types depending on its optical and electrical properties. Edwards and Philipp [45] have compiled spectral data for the natural types Ia and IIa and they concluded that the difference of the refractive index in the visible range is very small (less than 1%) between these types. In the Cauchy plot (Fig. 4), the
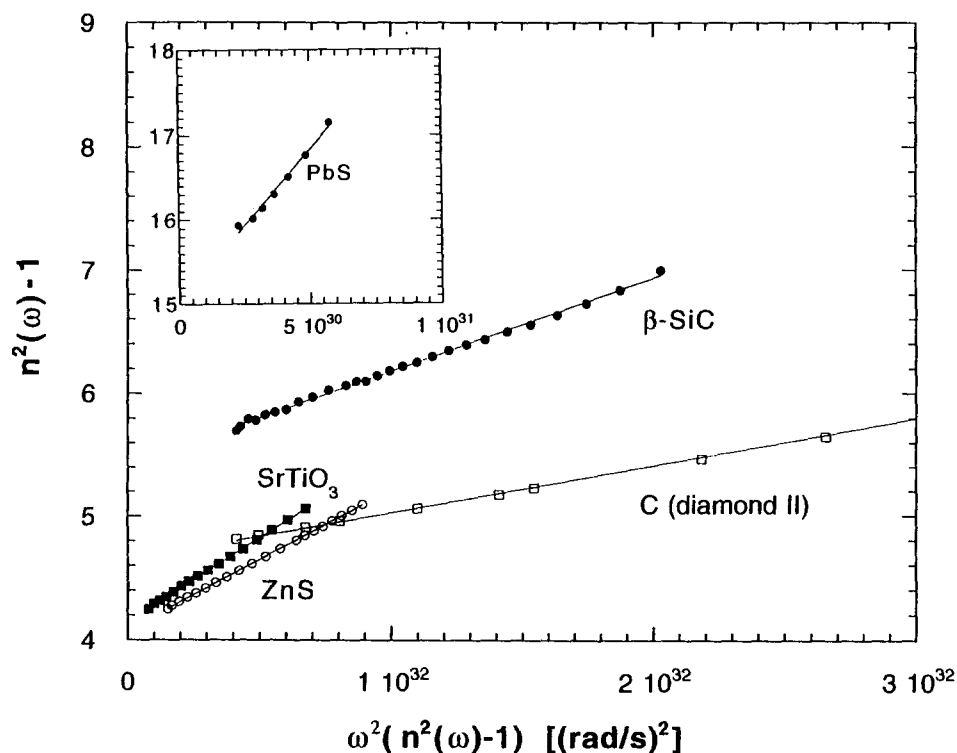
Fig. 4. Cauchy plots for the cubic materials: β-SiC, C (diamond type II), $SrTiO_3$, ZnS, and PbS (insert).

sparse refractive index data from Peter [46] was used. The infrared absorption is of minor importance since the absorption, and thus the C_{IR} value, is so low (Table 2). However, the value of the phonon frequency [47] was used for the characteristic frequency in the infrared.

2. PbS

Lead sulphide is a semiconductor having a cubic rock salt crystal structure. Guizzetti and Borghesi [48] have compiled the dielectric data, generally focusing on materials with low free carrier concentrations. Since lead sulphide displays significant absorption in the ultraviolet–visible frequency range, the Cauchy plot in Fig. 4 rests on some sparse data in the near-infrared, originating from Zemel et al. [49]. Fortunately, the infrared absorption band occurs at very low frequencies [50], leaving a sufficiently broad transparent frequency region for Cauchy treatment.

3. β-SiC

The spectroscopic ellipsometry data on cubic β-silicon carbide reported by Alterovitz and Woollam [51] was used in the Cauchy plot (Fig. 4). The spectral data of this material, which is of the zincblende structure, agree very well with reported values of n_0 for hexagonal 6H-silicon carbide [52]. The infrared absorption data are from Spitzer et al. [53].

4. SrTiO₃

Dielectric data on undoped strontium titanate single crystals of the cubic perovskite structure have been collected by Gervais [54]. The $n(\omega)$ data plotted in the Cauchy plot (Fig. 4) were taken from reflectivity measurements by Cardona [55]. The infrared absorption data are from Spitzer et al. [56].

5. ZnS

The natural crystal modifications of zinc sulphide include the cubic, zincblende, and the hexagonal, wurtsite type. Zinc sulphide minerals usually contain substantial amounts of impurities with iron being the principal one. These impurities affect the colour of the minerals with the purest minerals having a light yellow body colour [57]. Palik and Addamiano [57] have collected the dielectric data of both of the zinc sulphide forms, focusing on synthetic materials or pure minerals. The calculated refractive index values presented by Pikhtin and Yaskov [58] in the ultraviolet–visible frequency range for the cubic modification were used for the Cauchy plot in Fig. 4. Infrared data was taken from Deutsch [59].

IVD. Tetragonal, hexagonal and trigonal materials

In this section, the spectral parameters of tetragonal, hexagonal or trigonal materials with negligible or undetermined birefringence are reported. The spectral parameters of several polycrystalline ceramic materials were recently reported by Bergström et al. [6]. They used spectroscopic ellipsometry to determine $n(\omega)$ in the ultraviolet–visible spectral range and calculated the oscillator parameters from Cauchy plots (UV range). The spectral constant C_{IR} was determined from the static dielectric constant using Eq. (25). Their spectral parameters for polycrystalline hexagonal 6H-SiC and β-Si_3N_4, and tetragonal, partially stabilised ZrO_2(3% Y) are included in Table 2 with some slight modifications. The number of valid figures has been increased and a slightly lower value of $\varepsilon(0)$ for polycrystalline, hexagonal α-Al_2O_3 — which is the average value of $\varepsilon(0)$ for the ordinary and extraordinary ray — was used in this study. The spectral parameters of hexagonal yttrium oxide (Y_2O_3) were also collected from the study by Bergström et al. [6] using optical data from the literature.

Crystalline quartz (SiO_2) of the trigonal crystal structure displays a small birefringence, as analysed by Hough and White [10]. Only the average values are reported in Table 2. Senden and Drummond [26] have performed a thorough analysis of the dielectric data of muscovite mica which is a potassium aluminosilicate ($KAl_2Si_3AlO_{10}(OH)_2$) belonging to the monoclinic crystal class. They concluded that the spectral parameters in different crystallographic directions affect the calculated by no more than ±1%; hence, only the average values are reported in Table 2.

1. CdS

The semiconducting compound cadmium sulphide (CdS) is normally of the hexagonal close-packed (wurtzite) crystal structure but a cubic form may occur. Here, only the hexagonal form will be treated, summarised by Ward [60]. Data for both the ordinary and extraordinary rays are available but since the difference in dielectric response is negligible, data for polycrystalline CdS [61] in the ultraviolet–visible range was used for the Cauchy plot in Fig. 5. The infrared data was from Manabe et al. [62].

2. MgF₂

Magnesium fluoride (MgF_2) is an ionic, tetragonal material with rutile crystal structure. The dielectric data of this slightly birefringent material has been compiled by Cotter et al. [63]. Refractive index data
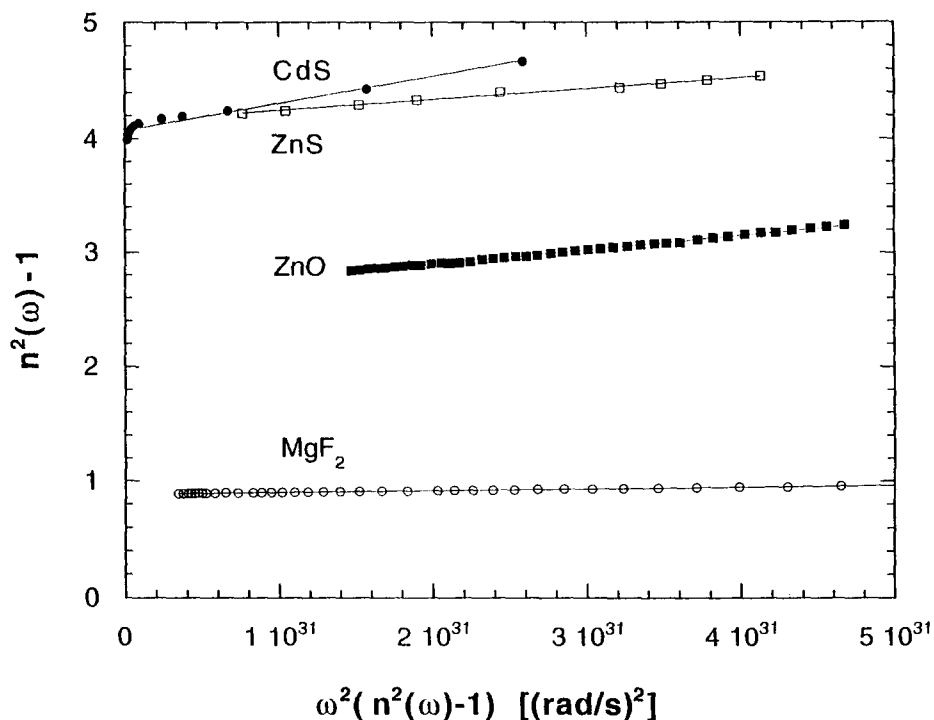
Fig. 5. Cauchy plots for tetragonal and hexagonal materials with negligible birefringence; CdS, MgF$_2$, ZnO, ZnS.

for the ordinary ray, presented in a fitted form by Dodge [64] was used for the Cauchy plot in Fig. 5. The infrared data was from Barker's compilation of IR modes [65].

3. ZnO

The optical data in the ultraviolet–visual range for polycrystalline, hexagonal zinc oxide (ZnO) was taken from the Fig. 2, previously reported by Bergström et al. [6]. Only the data in the transparent region, thus sufficiently below the band gap energy, was used for the Cauchy plot in Fig. 5. The infrared data was from Farmer [66].

4. ZnS

The optical data in the ultraviolet–visual spectral range for the hexagonal modification of zinc sulphide was taken from Bienewski and Czyzak [67]. The material only displays a minor birefringence in this transparent spectral region so only the ordinary ray data was used for the Cauchy plot (Fig. 5). The infrared data was from Manabe et al. [62]. Comparison of the spectral parameters for cubic and hexagonal zinc

sulphide show relatively small differences; hence, it is not critical to know the exact composition when estimating the Hamaker constant for a phase mixture, e.g. the commercially available IRTRAN 2 material.

IVE. Birefringent materials

Previous analysis of the dielectric data in different crystallographic orientations has shown that the trigonal material calcite ($CaCO_3$) and the tetragonal material rutile (TiO_2) display significant birefringence. The data for calcite from Hough and White [10] and the spectral parameters for rutile, recently reported by Buscall [68], are shown in Table 2.

1. $BaTiO_3$

The Cauchy plot for tetragonal $BaTiO_3$ having a perovskite crystal structure, is shown in Fig. 6. Spectral data have been collected by Wong
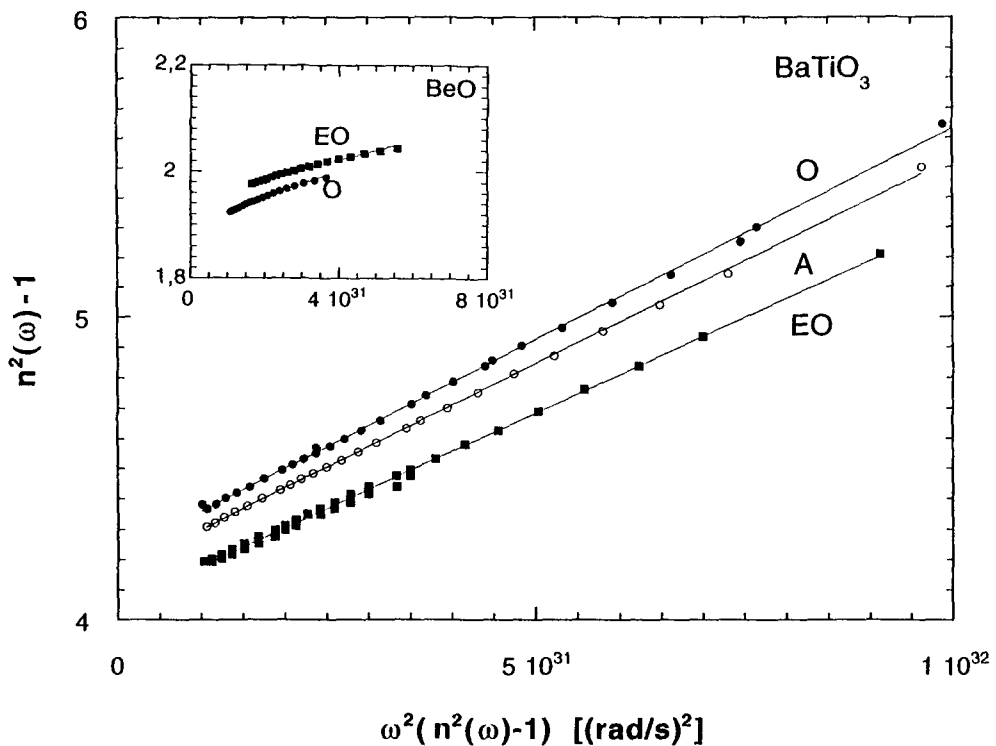
Fig. 6. Cauchy plots for the birefringent materials; tetragonal $BaTiO_3$, and inserted; hexagonal BeO. The ordinary (O) and extraordinary (EO) rays represent the refractive indices perpendicular and parallel to the optical axis, respectively. The averaged representation (A) can be obtained by $n_a = (1/3)n_{eo} + (2/3)n_o$.

et al. [69] and the optical properties of melt-grown single crystal $BaTiO_3$ [70] was used in the Cauchy plot. It can be seen that the optical anisotropy for this material is quite significant; the curves for the ordinary and extraordinary rays are well separated and there is a 4–6% difference in obtained spectral parameters for the two crystallographic orientations. The average representation for the ultraviolet–visible spectral range was obtained by adding one third of the c-axis (extraordinary) contribution and two thirds of the a-axis (ordinary) contribution following rationale above. The infrared and static spectral parameters will be discussed in detail later.

2. BeO

The relatively sparse optical data for hexagonal beryllium oxide (BeO) have been collected by Edwards and White [71]. The data from Newkirk et al. [72] was used for the Cauchy plot (insert in Fig. 6). The optical anisometry is quite significant also for this material, in particular regarding the ω_{UV} where a 20% difference between the two crystallographic orientations was found. The infrared data was from Loh [73].

V. Calculated Hamaker constants

VA. Importance of the IR range.

The importance of the IR range for the calculation of Hamaker constants was tested for two materials: $BaTiO_3$ which is characterised by a very high $\varepsilon(0)$, and thus a high C_{IR}, and SiO_2 which has a low $\varepsilon(0)$. Full Lifshitz calculations, using Eq. (19), were performed across three different media: vacuum, water and n-dodecane; investigating the effect of the infrared contribution. The calculated values collected in Table 3 show that the IR contribution to the Hamaker constant is significant for $BaTiO_3$ in all media; for SiO_2 the IR contribution is negligible except in the case of n-dodecane where the C_{UV} and ω_{UV} of the medium and the material are very similar resulting in a very low UV contribution to the non-retarded Hamaker constant. Hence, for a material characterised by a relatively low value of C_{IR}, like most ceramic materials, the IR contribution to the Hamaker constant is very small, typically only a few percent, except in the case when the intervening medium has a similar dielectric response function in the UV range as the material.

In the case of a material characterised by a high C_{IR} and sufficiently high ω_{IR}, e.g. $BaTiO_3$, the IR contribution is significant irrespective of

Table 3

Non-retarded Hamaker constants for tetragonal $BaTiO_3$ and silica interacting across vacuum, water and n-dodecane at room temperature (298 K)

Material	Medium		
	Vacuum	Water	n-dodecane
$BaTiO_3$			
ω_{IR} (10^{14} rad/s)		Hamaker constant (10^{-20} J)	
–	14.1	4.45	3.77
0.7	17.6	7.91	7.44
1.0	19.3	9.49	8.99
SiO_2			
ω_{IR} (10^{14} rad/s)		Hamaker constant (10^{-20} J)	
–	6.35	0.48	0.097
See Table 2 (3 IR contributions)	6.50	0.46	0.14

the dielectric properties of the medium. With water or n-dodecane as the intervening media, the IR contribution attributes for more than 50% of the total value of the non-retarded Hamaker constant, thus making an accurate dielectric representation of the infrared range important. In the case of $BaTiO_3$, Wemple et al. [70] reported room temperature dielectric constants measured at 100 kHz of: $\varepsilon_a = 3600$, $\varepsilon_c = 150$. The average static dielectric constant was estimated as $\varepsilon_{aver} = 2400$. Busca et al. [74] have studied the IR characteristics of a tetragonal $BaTiO_3$ powder. They found that the IR spectrum has two dominant complex absorptions: one in the region 600–500 cm^{-1} and the other in the region 450–350 cm^{-1}. These absorptions correspond to ω_{IR} at 1.0×10^{-14} and 0.7×10^{-14} rad/s, respectively. With the uncertainty in the IR absorption frequency, the error in the Hamaker constant becomes relatively large. A reasonable estimate of the non-retarded Hamaker constant for tetragonal $BaTiO_3$ in vacuum is $18 \pm 1.5 \times 10^{-20}$ J, across water $A_{1w1} = 8 \pm 1.5 \times 10^{-20}$ J, and across n-dodecane $A = 7.5 \pm 1.5 \times 10^{-20}$ J. Hence, for such a material with a significant IR contribution, the error in the Hamaker constant calculation becomes relatively large (10–20%) using the present representation. The accuracy of the calculations may be improved using a more detailed IR representation.

Table 4

Non-retarded Hamaker constants in vacuum and across water for inorganic materials

Material	Crystal structure	Hamaker constants (10^{-20} J)			
		Vacuum (air)		Water	
		Full Lifshitz	TWS approx.*	Full Lifshitz	HIS approx.**
α-Al$_2$O$_3$	hexagonal	15.2	14.8	3.67	4.72
BaTiO$_3$ (average)	tetragonal	18	13.9	8	5.24
BeO (average)	hexagonal	14.5	14.2	3.35	4.35
C (diamond IIa)	cubic	29.6	28.5	13.8	15.5
CaCO$_3$ (average)	trigonal	10.1	9.43	1.44	1.78
CaF$_2$	cubic	6.96	6.88	0.49	0.84
CdS	hexagonal	11.4	11.0	3.40	3.89
CsI	cubic	8.02	7.93	1.20	1.54
KBr	cubic	5.61	5.58	0.55	0.63
KCl	cubic	5.51	5.48	0.41	0.51
LiF	cubic	6.33	6.24	0.36	0.64
MgAl$_2$O$_4$	cubic	12.6	12.3	2.44	3.28
MgF$_2$	tetragonal	5.87	5.83	0.37	0.59
MgO	cubic	12.1	11.8	2.21	2.96
Mica	monoclinic	9.86	9.64	1.34	1.93
NaCl	cubic	6.48	6.43	0.52	0.74
NaF	cubic	4.05	4.01	0.31	0.26
PbS	cubic	8.17	7.81	4.98	4.82
6H-SiC	hexagonal	24.8	23.8	10.9	12.1
β-SiC	cubic	24.6	23.6	10.7	11.9

Material	Crystal structure	Hamaker constants (10^{-20} J)			
		Vacuum (air)		Water	
		Full Lifshitz	TWS approx.*	Full Lifshitz	HIS approx.**
β-Si$_3$N$_4$	hexagonal	18.0	17.4	5.47	6.57
Si$_3$N$_4$	amorphous	16.7	16.2	4.85	5.90
SiO$_2$ (quartz)	trigonal	8.86	8.64	1.02	1.51
SiO$_2$ (silica)	amorphous	6.50	6.39	0.46	0.71
SrTiO$_3$	cubic	14.8	13.9	4.77	5.10
TiO$_2$ (average)	tetragonal	15.3	14.3	5.35	5.65
Y$_2$O$_3$	hexagonal	13.3	13.0	3.03	3.85
ZnO	hexagonal	9.21	8.98	1.89	2.24
ZnS	cubic	15.2	14.8	4.80	5.65
ZnS	hexagonal	17.2	16.6	5.74	6.73
3Y-ZrO$_2$	tetragonal	20.3	19.3	7.23	8.13

* Values using the TWS (Tabor–Winterton including the static contribution) approximation were calculated using Eq. (21).

** The HIS (Horn–Israelachvili including the static contribution) approximation uses Eq. (22) for the dispersive contribution and the same expression for the static contribution as in the TWS approximation. Values for $\varepsilon(0)$, n, and ω_{UV} for water were taken from Prieve and Russel [19].

VB. Full Lifshitz calculations and analytical approximations

Non-retarded Hamaker constants were calculated for all the symmetric systems, material 1 interacting across a medium 3, using full Lifshitz calculations, Eq. (19), across vacuum and water. Non-retarded Hamaker constants were also estimated using two different approximations, Eq. (21) for the Hamaker constant in vacuum (Tabor–Winterton equation including the static contribution (TWS)), and Eq. (22) together with the static term in Eq. (21) (Horn–Israelachvili (HIS) equation) for the Hamaker constant across water. The calculated values are collected in Table 4. The non-retarded Hamaker constants in vacuum, A_{1v1}, vary between 296 zJ (1 zJ = 10^{-21} J) for diamond down to 40.5 zJ for NaF. Most of the halides have relatively low non-retarded Hamaker constants while the more covalently bonded oxides, carbides and nitrides have significantly higher values. The TWS approximation gave a surprisingly good correspondence to the full Lifshitz calculations. It should be observed that for these calculations, the appropriate ω_{UV} and n_0 for each material (from Table 2) were used. The average error for the 31 inorganic materials were only $\approx 3\%$, except for $BaTiO_3$ where the TWS approximation predicts a value 23% too low. The main difference between the TWS approximation and the full Lifshitz calculation is that the TWS approximation only considers the contribution from the UV-vis region, hence ignoring the IR contribution to $\varepsilon(i\xi)$, and that the double summation in Eq. (19) is approximated with an analytical expression. The good agreement between the full Lifshitz and the TWS approximation supports the previous statement that the IR contribution to the non-retarded Hamaker constant is negligible for most ceramic materials in vacuum or air. This is an encouraging result since it was difficult to obtain detailed information of the IR absorption behaviour for some of the materials. A smaller error in ω_{IR} and C_{IR} should not result in any significant change in the estimated value of A_{1v1}.

With water as the intervening medium, there is a much larger spread in the non-retarded Hamaker constants, A_{1w1}; from 3.1 zJ for NaF to 138 zJ for diamond. All these calculation were performed using the new spectral representation of water [13], see Table 1. In general, the non-retarded Hamaker constants presented here are significantly lower than earlier estimates using the previous, less exact, UV representations of water. For example, the non-retarded Hamaker constants across water Hough and White [10] calculated for silica (8.49 zJ), calcite (22.3 zJ), calcium fluoride (10.4 zJ) and sapphire (53.2 zJ) are up to two

times larger than the values calculated in this study. Similarly, the non-retarded Hamaker constants across water presented by Bergström et al. [6] for nine different inorganic materials are significantly larger than the present values. One material where the magnitude of the vdW interaction is of special importance is muscovite mica; an extensively used material in direct surface force measurements [1,22,75]. Commonly used values for A_{1w1}(mica) = 20 ± 2 zJ [1,26] are almost 50% higher compared to the present value of A_{1w1}(mica) = 13.4 zJ. A lowering of the Hamaker constant for this system may have important implications regarding the interpretation of the obtained force curves.

There is a relatively poor correspondence between the full Lifshitz calculations and the HIS approximation across water. The HIS approximation, which utilises only one value for ω_{UV} and C_{UV} for the material and the medium, respectively, appears to overestimate the Hamaker constant across water for almost all the materials while the TWS approximation underestimates the non-retarded Hamaker constant in vacuum. Note that the TWS approximation can not be used for calculations with an intervening medium since the inherent assumption of a common ω_{UV} for the material and the medium never holds. Depending on the spectral parameters of the materials, the HIS approximation overestimates the non-retarded Hamaker constant with almost a factor of two. While the underestimation in the TWS case can be explained by the absence of the IR range contribution, the overestimation using the HIS approximation across water is probably due to the poor spectral representation of water using only one UV oscillation. For media with simpler spectral features, e.g. dodecane, a very good correspondence between the full Lifshitz calculations and the HIS approximation is obtained (not shown).

VC. Hamaker constants for use in AFM studies

The use of atomic force microscopy (AFM) to probe the distance dependent forces between various materials separated by air, vacuum or liquids have recently gained much interest. Initially, the forces between the cantilever tip — typically made of silicon nitride — and a substrate, commonly mica, was monitored and manipulated [75–79]. This work has been extended by measuring the force curves between silicon nitride tips and substrate in liquids at different conditions [26,80,81], and attaching colloidal spheres of different materials to the AFM cantilevers [82–85]. These developments have made AFM a versatile

tool for studying the complex interactions between surfaces of different materials.

To assist the interpretation of AFM force measurements, the non-retarded Hamaker constants of materials interacting across vacuum (air) and water against four materials: silica, amorphous silicon nitride, sapphire (α-Al_2O_3), and muscovite mica have been calculated (Table 5). These materials are commonly used either as cantilever tips (silicon nitride), colloidal probes (silica) or inorganic substrates (sapphire, mica) in AFM studies. In general, the magnitude of the Hamaker constants follows the expected trends with a large value for high refractive index

Table 5

Non-retarded Hamaker constants in vacuum and across water (vacuum/water) of inorganic materials interacting against four materials at room temperature

| Material | Hamaker constant (10^{-20} J) | | | |
	Silica	Silicon nitride	Alumina	Mica
$BaTiO_3$	10.1/0.62	16.5/4.84	15.2/3.55	12.4/1.98
BeO	9.67/0.95	15.4/3.87	14.8/3.50	11.9/2.06
C (diamond)	13.7/1.71	22.0/7.94	21.1/7.05	17.0/4.03
$CaCO_3$	8.07/0.69	12.9/2.53	12.3/2.17	9.94/1.35
CaF_2	6.70/0.45	10.6/1.17	10.3/1.10	8.26/0.73
CdS	8.03/0.72	13.1/3.12	12.0/2.15	9.86/1.43
KCl	5.94/0.37	9.53/0.73	9.00/0.51	7.31/0.46
$MgAl_2O_4$	9.05/0.85	14.5/3.39	13.8/2.97	11.2/1.79
MgF_2	6.15/0.36	9.74/0.66	9.42/0.69	7.57/0.50
MgO	8.84/0.81	14.2/3.26	13.5/2.79	10.9/1.69
Mica	8.01/0.69	12.8/2.45	12.2/2.15	9.86/1.34
NaCl	6.45/0.44	10.3/1.17	9.77/0.88	7.93/0.66
PbS	5.37/−0.08	8.88/0.64	7.90/−0.20	6.57/−0.03
6H-SiC	12.6/1.52	20.3/7.22	19.2/6.05	15.5/3.54
β-Si_3N_4	10.8/1.17	17.3/5.13	16.5/4.43	13.3/2.61
SiO_2 (quartz)	7.59/0.63	12.1/2.07	11.6/1.83	9.35/1.16
$SrTiO_3$	9.44/0.57	15.4/4.02	14.2/2.98	11.6/1.69
TiO_2	9.46/0.69	15.4/4.26	14.2/3.11	11.6/1.83
Y_2O_3	9.24/0.89	14.9/3.80	14.0/3.11	11.4/1.89
ZnO	7.38/0.58	12.0/2.30	11.1/1.58	9.06/1.08
ZnS (cubic)	9.69/1.02	15.7/4.56	14.6/3.55	11.9/2.19
3Y-ZrO_2	11.4/1.25	18.4/5.89	17.4/4.95	14.1/2.89

material like silicon nitride and a lower value for a low refractive index material like silica. In vacuum, the non-retarded Hamaker constants span is relatively narrow: from 53.7 zJ (PbS against silica) to 220 zJ (diamond against silicon nitride). With water as the intervening medium, the magnitude of the van der Waals attraction is of course reduced and also broadened depending on the material: from 3.7 zJ (KCl against silica) to 79.4 zJ (diamond against silicon nitride).

In fact, negative non-retarded Hamaker constants, indicating a repulsive van der Waals interaction, were calculated for several material combinations involving PbS across water. A negative Hamaker constant represents a destructive electrodynamic interaction between the materials and it is only recently that direct measurements of repulsive van der Waals forces were demonstrated [86,87]. In general, repulsive van der Waals forces are predicted for systems where the magnitude of the dielectric response of the medium is intermediate to the magnitude of the dielectric response of the two different interacting materials. For PbS, having the spectral characteristics of a very high $\varepsilon(0)$, extremely high n_0 (or C_{UV}), and a very low ω_{UV}, the calculations against the four materials across water (Table 5) display several interesting features.

The static contribution ($m = 0$) is negative (repulsive) for all these material combinations since $\varepsilon(0)$ of the medium (water) is intermediate to $\varepsilon(0)$ for PbS and the materials. Since the static contribution usually is of minor importance, it is of interest to analyse the dispersive contribution in some detail. However, it should be noted that the spectral parameters in the UV–visible spectral range for PbS relies on relatively sparse data, thus making the spectral representation less accurate. As illustrated in Fig. 7 for two of the materials combinations: PbS against silica, and PbS against silicon nitride, the dispersive contribution changes sign from positive to negative above a critical frequency. Hence, in the infrared and visible part of the spectrum ($m < 25$), the interaction is constructive while the contribution from the ultraviolet region ($m > 25$) is destructive. In the system silica against PbS, this balance is very delicate resulting in a very small, positive dispersive contribution (0.2 zJ) to the non-retarded Hamaker constant when the contributions from all the frequencies have been summated. Since the static contribution (–1.0 zJ) dominates the total van der Waals interaction for this system, the calculations suggests that screening this interaction, e.g. by addition of salt [2], would result in a system with a negligible vdW attraction.
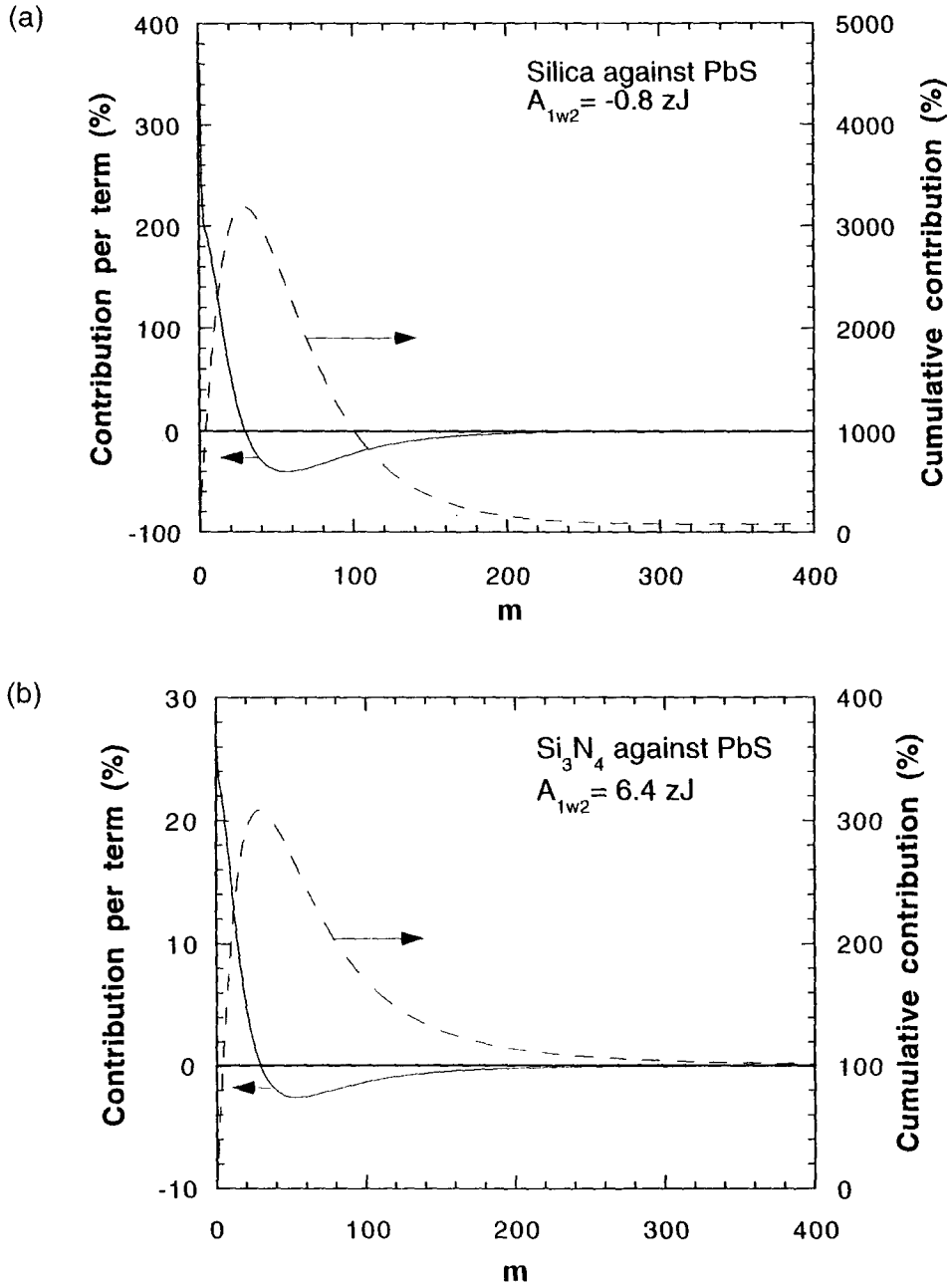
Fig. 7. Contributions from individual terms in Eq. (19) of the dispersive part ($m > 0$) to the non-retarded Hamaker constants, A_{1w2} for PbS against (a) silica, and (b) silicon nitride, across water. The static contribution was –1.0 zJ, and –0.9 zJ for (a) and (b), respectively.

VD. Spectral parameter scalings

With the absence of detailed spectroscopic data, we are limited to the simplified expressions for calculating non-retarded Hamaker constants. The TWS and HIS approximations are examples of such simplifications. However, even for the simple TWS approximation of the non-retarded Hamaker constant in vacuum, we have to know three parameters: ω_{UV}, n_0, and $\varepsilon(0)$. Usually, values of the refractive index in the visible and the static dielectric constant can be found for most materials but ω_{UV} is usually not tabulated and has to be extracted from data of the frequency dependence of the refractive index which may be hard to find. Without such data, the assumption originating from Tabor and Winterton [22] of a common value of $\omega_{UV} \approx 2 \times 10^{16}$ rad/s for all materials is frequently used.

Figure 8 illustrates how a common value of $\omega_{UV} \approx 2 \times 10^{16}$ rad/s results in a systematic overestimation of the non-retarded Hamaker constants for many of the inorganic materials. For simplicity, the original Tabor–Winterton (TW) approximation was used, thus not including the static contribution which is negligible for vdW interactions across vacuum. The deviation of the Lifshitz value for A_{1v1} from this simplified TW
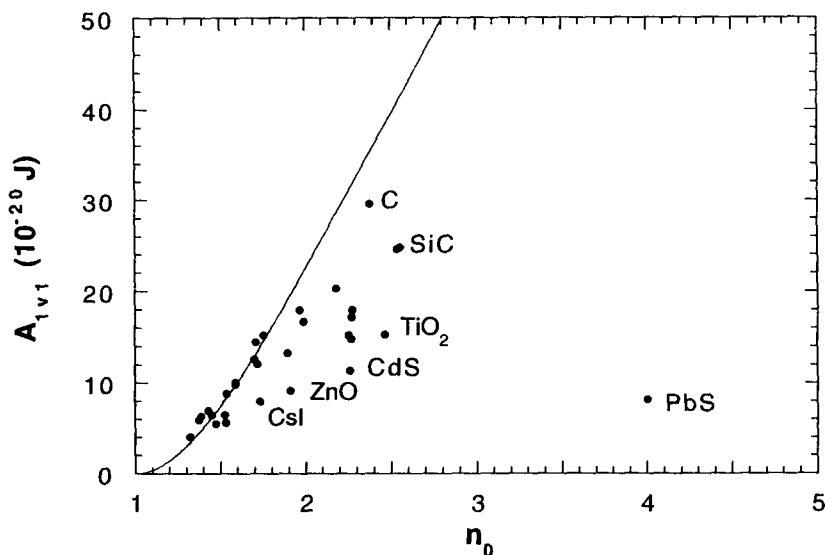
Fig. 8. Non-retarded Hamaker constants for inorganic materials across vacuum (A_{1v1}) versus the limiting refractive index, n_0, from Table 2. Solid line denotes the TW approximation with $\omega_{UV} = 2 \times 10^{16}$ rad/s.

approximation increases with increasing refractive index. This agrees with previous studies [7,88] which concluded that the TW approximation results in poor correspondence to full Lifshitz calculations for high refractive index materials. However, this does not reflect any significant inherent errors in the TWS approximations; it merely relates to a poor choice of ω_{UV}. If the appropriate values of the spectral parameters, in particular ω_{UV}, are used, the results in Table 4 clearly show that the TWS approximation gives quite accurate results when compared to full Lifshitz calculations for most materials.

The relation between the refractive index, n_0, and ω_{UV} is shown in Fig. 9. All the materials display a decreasing ω_{UV} with an increasing refractive index which can explain the increasing deviation in the value of A_{1v1} between the full Lifshitz calculations and the TW approximation using a constant value of ω_{UV}. An attempt was made to establish a general scaling relation for all these materials. Due to the large scatter of the data in Fig. 9a, however, it was not possible to describe all the different materials with such a scaling relation. If we somewhat arbitrarily limit the data to covalent oxides, sulphides and nitrides, thus excluding the ionic halides, and SiC and diamond, a simple scaling relation at higher refractive indices, following the power law

$$\omega_{UV} = \frac{8.8 \times 10^{16}}{n^{2.8}} \tag{26}$$

may be established, although a significant scatter of the data still remains (Fig. 9b). Figure 9b indicates that for covalent materials with a low refractive index ($n_0 < 1.7$), ω_{UV} appears to be independent of n_0. A simple scaling between the refractive index in the visible and the non-retarded Hamaker constant has been illustrated previously by Buscall [68] for materials such as polymers, hydrocarbons, quartz and calcite. The success of this scaling can be referred to the nearly identical ω_{UV} of these low refractive index materials. Buscall also concluded that such a correlation is not applicable when ω_{UV} deviates substantially from this common value, as observed with rutile, a high refractive index

Opposite: Fig. 9. Relation between the characteristic frequency in the UV range, ω_{UV}, and the refractive index in the visible, n_0: (a) all the inorganic materials, (b) only the covalent materials thus excluding the halides. The high refractive index materials, diamond and silicon carbide have also been excluded in (b) where the full line represents the power law fit according to Eq. (26).
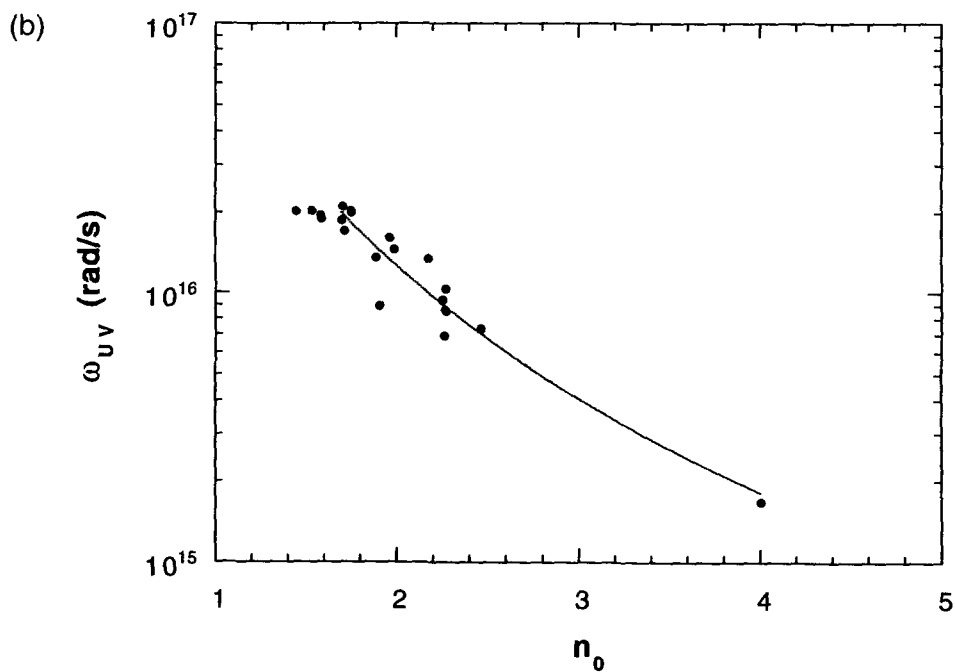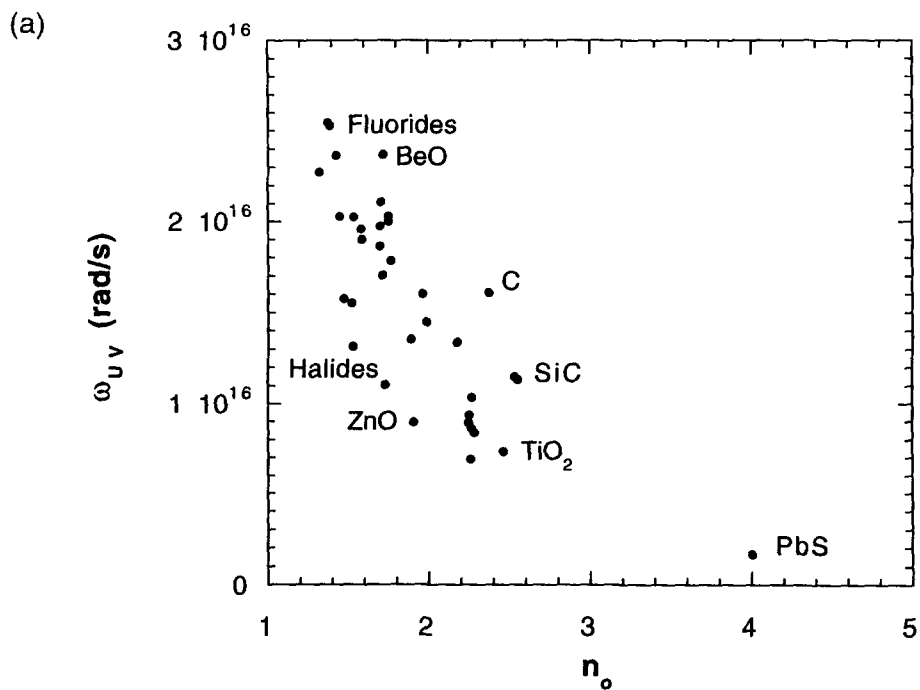
material ($n = 2.46$). In this work, however, no attempt to implement the scaling in Eq. (26) in the TWS approximation was made due to the large scatter of the data.

VE. Comparison with a Kramers–Kronig dielectric representation

French and co-workers [7,88] have recently published several papers where the non-retarded Hamaker constants of ceramic materials have been calculated using a slightly different scheme applying the integral form of the Hamaker constant expression (Eq. (20)). The imaginary dielectric representation, $\varepsilon(i\xi)$, of the materials were obtained through Kramers–Kronig transformations of experimentally determined interband transition strengths over a relatively wide photon energy range (0.46 to 44 eV) from optical reflectivity spectra. Non-retarded Hamaker constants for different combinations were calculated using a commercially available collection of the necessary programs and a spectral data base of many materials. As previously stated, the accuracy of Hamaker constants calculated from Lifshitz theory relies on the quality of the experimental dielectric data and the accuracy of the spectral representation. Since French and co-workers [7,88] use dielectric data over a wide frequency range, their method has the potential of obtaining a very detailed spectral representation in the important frequency range. In principle, the N–P representation has the same potential if a sufficient number of relaxations is introduced. Of course, accurate dielectric representations can only be obtained from accurate dielectric data.

Ackler et al. [88] recently presented data on non-retarded Hamaker constants calculated by the method described above, using the integral equation and Kramers–Kronig relations (IKK method), and compared their values with previously published values where the method in this study, the summation equation (Eq. (19)) with an N–P dielectric representation (SNP method) was used. Also, other simplified models were used for 5 different materials: muscovite mica, Al_2O_3, SiO_2, Si_3N_4, and rutile TiO_2, separated by vacuum and water. In the IKK calculations [88], the dielectric representation for the inorganic materials was obtained from VUV reflectivity data as described above while the $\varepsilon(i\xi)$ function for water was determined from literature data [12] and K–K transformed to be incorporated in the data base.

Here, their values for the non-retarded Hamaker constants using the IKK method are compared with values using the SNP method (Table 6) in an attempt to assess the accuracy of representing the materials with

Table 6

Comparison of calculated non-retarded Hamaker constants using two different methods: the integral Kramers–Kronig (IKK) method and the summation Ninham–Parsegian (SNP) method

Material	Hamaker constant (10^{-20} J)				
	Vacuum		Water		
	IKK [88]	SNP	IKK [88]	SNP	SNP-UV*
Mica	6.96	9.86	0.29	1.34	1.08
Al_2O_3	14.5	15.2	2.75	3.67	3.48
SiO_2	6.60	6.50	0.16	0.46	0.17
Si_3N_4	17.4	18.0	4.6	5.47	5.22
TiO_2 rutile	17.3	15.3	6.0	5.35	5.02

* SNP-UV calculations were performed using Eq. (19) including only the UV contribution of the $\varepsilon(i\xi_m)$ function of both the materials and water.

the simplified, two oscillator, N–P representation. Observe that the values for the non-retarded Hamaker constants using the SNP method differs in this study and in Ackler et al. [32] since a new water representation is used here. With vacuum as the intervening media, there is a very good correspondence of the calculated values of A_{1v1} for three of the materials: alumina, silica, and silicon nitride, with an average difference of only 3%. For mica, the IKK method yields a significantly lower value while the IKK method yields a 12% higher value of the Hamaker constant for rutile. The difference in the calculated values between the two methods is increased significantly for the non-retarded Hamaker constants across water.

There are two main differences between the IKK and the SNP methods. In the IKK method, the integral equation for the non-retarded Hamaker constant is used (Eq. (20)) which ignores the static contribution. The SNP method uses the double summation equation which includes this contribution, referring to the first summation ($m = 0$) in Eq. (19). The IKK method typically has an imaginary dielectric representation over a significantly broader frequency range, in particular the high frequency range, compared to the simplified N–P representation using only one UV and possibly a few IR terms (Eq. (14)). The IKK

method, however, also ignores the IR contribution at present [7]. It is of interest to evaluate the effect and magnitude of these two differences between the IKK and SNP method. Unfortunately, such a comparison is complicated by the fact that dielectric data of different origin was used for most materials. Hence, the difference in the calculated values of the non-retarded Hamaker constants can be caused by either the difference in mathematical treatment (integral and summation), the accuracy of the original dielectric data (frequency dependence of the refractive index or interband transition strengths) and using an appropriate imaginary dielectric representation.

Ignoring the static and low frequency contribution of the $\varepsilon(i\xi)$ representation will only have a marginal effect on the non-retarded Hamaker constant for materials interacting across vacuum since the dispersive part completely dominates the value of A_{1v1}. The static contribution is usually of minor importance in all systems since its maximum value is 0.75 kT (4.1 zJ at room temperature) but it can have a significant influence at high temperatures or when the dispersive part of the Hamaker constant is very small. The significance of the IR contribution was discussed previously and no major influence is expected except for materials with very high values of the static dielectric constant. Hence, since no major differences are expected using the integral or the summation equations (Eqs. (20) and (19), respectively) for low $\varepsilon(0)$ materials in vacuum, the nearly identical values of A_{1v1} for Al_2O_3, SiO_2 and Si_3N_4 suggests that the dielectric representations are similar in the two studies. This is supported by the close correspondence of the index of refraction ($\Delta n < 0.05$) for these materials in Ackler et al. [32] and in this work. For rutile, the higher A_{1v1} using the IKK method may be explained by a difference in the original dielectric data, Ackler et al. [32] reporting $n = 2.6$ while this study uses $n = 2.46$ based on data from Buscall [68]. For mica, a similar explanation may apply, or the significantly lower A_{1v1} value using the IKK method may be related to the fine details of the $\varepsilon(i\xi)$ representation over a wider frequency range.

Turning to the non-retarded Hamaker constants across water, there is a significant difference in A_{1w1} between the two methods for all materials. The IKK method always yields lower values compared to the SNP method. In water, the dispersive contribution becomes very small for some materials, thus making the static and low frequency contribution important. For silica, the result in Table 6 shows that the difference between the two methods can be fully related to the omission of this contribution in the IKK method. For all the other materials, except mica,

the difference between the IKK and SNP-UV (omitting static and IR contribution) was less than 30%. The large difference in A_{1w1} for mica, almost a factor of four, must be related to major differences in the imaginary dielectric representation, either due to major differences in the original dielectric data or to the capability of the IKK method to yield a detailed $\varepsilon(i\xi)$ representation over a wide frequency range. In summary, a comparison of these two methods suggests that the simplified N–P representation over a limited frequency range in general yields non-retarded Hamaker constants which do not differ significantly from calculations using a more detailed representation over a broader frequency range. This is not true for all materials, e.g. water, where a more detailed representation using either an N–P representation with several oscillators or the K–K representation. It is possible that mica also is such a material.

VI. Summary and conclusions

Calculation of non-retarded Hamaker constants from Lifshitz theory relies on the accuracy of the dielectric spectral representation and the quality of the experimental dielectric data of the materials and media. In this review, spectral parameters for 31 different inorganic materials (including diamond) have been generated from critically evaluated optical data [11,12] or collected from different sources. The spectral parameters: the oscillator strengths and characteristic frequencies in the UV and IR range; C_{UV}, ω_{UV}, and C_{IR}, ω_{IR}, respectively, and the static dielectric constant, $\varepsilon(0)$, for the different inorganic materials generated here can be combined with previous data, mainly focused on hydrocarbon and organic systems [10], to yield an extensive spectral data base for both solids and liquids.

Non-retarded Hamaker constants across vacuum and water have been calculated using Lifshitz theory for the different inorganic materials (including diamond). All the symmetric combinations (material 1 against material 1) have been treated and the asymmetric combinations with most of the materials against silica, silicon nitride, alumina and mica. These calculations were performed using the full Lifshitz theory utilising the Ninham–Parsegian representation of the imaginary dielectric response function for the materials and medium. A recently reported improved spectral parametric representation of water [13] was used for these calculations which resulted in some significant changes in the value for A_{1w1}, e.g. for mica, compared to previous studies.

The full Lifshitz calculations were compared with various analytical simplifications and an alternative Lifshitz method. When the appropriate values of ω_{UV} and n_0 were used, a surprisingly good agreement was found — with vacuum as the intervening medium — between the full treatment and the Tabor–Winterton (TWS) approximation. The correspondence between the full Lifshitz treatment and the TWS approximation suggested that the IR frequency range of the dielectric representation is of minor importance for most materials. This was corroborated by a separate evaluation showing that the IR contribution to the non-retarded Hamaker constant is significant only for materials, like $BaTiO_3$, which are characterised by a very high static dielectric constant.

The calculations in this study utilising the Ninham–Parsegian representation of the dielectric data (SNP method) were compared with an alternative method ignoring the static and low frequency contribution and using the Kramers–Kronig transformation for the visible–UV range (IKK method). In general, the SNP method using a simplified N–P representation yields non-retarded Hamaker constants which do not differ significantly from calculations using the IKK method containing a more detailed dielectric representation over a broader frequency range. However, this is not true for all materials, e.g. water, where a more detailed representation using either an N–P representation with several relaxations or the K–K representation must be used. It is possible that mica is also such a material which implies that the more detailed dielectric representation of the IKK method should yield a more accurate value of the non-retarded Hamaker constant for this material. It should be noted that the values for A_{1w1} calculated for mica using the SNP (13.4 zJ) and the IKK method (2.9 zJ) are significantly lower than experimentally determined values using the surface force apparatus (22 zJ). Using silica as an example, it was shown that the omission of the static and low frequency contribution in the IKK method may result in a significant underestimation of the value for A_{1w1} when the dispersive contribution becomes very small.

Acknowledgements

References

[1] J. Israelachvili, Intermolecular and Surface Forces, 2nd edn. Academic Press, London, 1992.

[2] W.B. Russel, D.A. Saville and W.R. Schowalter, Colloidal Dispersions. Cambridge University Press, Cambridge, 1989.

[3] L. Bergström, in: R.J. Pugh and L. Bergström (eds.), Surface and Colloid Chemistry in Advanced Ceramics Processing. Marcel Dekker, New York, 1994, pp. 193.

[4] A. Bleier, J. Phys. Chem., 87 (1983) 3493.

[5] D.R. Clarke, J. Am. Ceram. Soc., 70 (1987) 15.

[6] L. Bergström, A. Meurk, H. Arwin, and D.J. Rowcliffe, J. Am. Ceram. Soc., 79 (1996) 339.

[7] R.H. French, R.M. Cannon, L. K. DeNoyer, and Y.-C. Chiang, Solid State Ionics, 75 (1995) 13.

[8] H.C. Hamaker, Physica, 4 (1937) 1058.

[9] E.M. Lifshitz, Sov. Phys. JETP, 2 (1956) 73.

[10] D.B. Hough and L.R. White, Adv. Colloid Interface Sci., 14 (1980) 3.

[11] E.D. Palik, Handbook of Optical Constants of Solids. Academic Press, Orlando, FL, 1985.

[12] E.D. Palik, Handbook of Optical Constants of Solids II. Academic Press, New York, 1991.

[13] C.M. Roth and A.M. Lenhoff, J. Colloid Interface Sci., 179 (1996) 637.

[14] V.A. Parsegian and B.W. Ninham, Nature, 224 (1969) 1197.

[15] B.W. Ninham and V.A. Parsegian, Biophys J., 10 (1970) 646.

[16] H. Krupp, Adv. Colloid Interface Sci., 1 (1967) 111.

[17] H. Krupp, W. Schnabel and J. Walter, J. Colloid Interface Sci., 39 (1972) 421.

[18] J. Mahanty and B.W. Ninham, Dispersion Forces. Academic Press, London, 1976.

[19] D.C. Prieve and W.B. Russel, J. Colloid Interface Sci., 125 (1988) 1.

[20] V.A. Parsegian, in: H. van Olphen and K.J. Mysels (eds.), Physical Chemistry: Enriching Topics from Colloid and Surface Science. Theorex, La Jolla, CA, 1975.

[21] J.M. Heller Jr., R.N. Hamm, R.D. Birkhoff and L.R. Painter, J. Chem. Phys., 60 (1974) 3483.

[22] D. Tabor and R.H.S. Winterton, Proc. R. Soc. London A, 312 (1969) 435.

[23] R.G. Horn and J.N. Israelachvili, J. Chem. Phys., 75 (1981) 1400.

[24] T. Shiosaki, in: A.S. Bhalla, E.M. Vogel and K.M. Nair (eds.), Ceramics Transactions, Vol. 14, Electro-Optics and Nonlinear Optic Materials. American Ceramic Society, Westerville, OH, 1990, pp. 197.

[25] K.F. Young and H.P.R. Friedrikse, J. Phys. Chem., Ref. Data, 2 (1973) 313.

[26] T.J. Senden and C.J. Drummond, Colloids Surfaces A: Physicochem. Eng. Aspects, 94 (1995) 29.

[27] D.F. Bezuidenhout, in Ref. [12], p. 815.

[28] I.H. Malitson, Appl. Opt., 2 (1963) 1103.

[29] W. Kaiser, W.G. Spitzer, R.H. Kaiser and L.E. Horwarth, Phys. Rev., 127 (1962) 1950.

[30] J.E. Eldridge, in Ref. [12], p. 853.

[31]　H.H. Li, J. Phys. Chem. Refer. Data, 5 (1976) 329.
[32]　J.A.B. Beairsto and J.E. Eldridge, Can. J. Phys., 51 (1973) 2550.
[33]　E.D. Palik, in Ref. [12], p. 989.
[34]　H.H. Li, J. Phys. Chem. Refer. Data, 5 (1976) 345.
[35]　K.W. Johnson and E.E. Bell, Phys. Rev., 187 (1969) 1044.
[36]　E.D. Palik, in Ref. [11], p. 703.
[37]　E.D. Palik and W.R. Hunter, in Ref. [11], p. 675.
[38]　H.H. Li, J. Phys. Chem. Ref. Data, 9 (1980) 561.
[39]　A. Kachare, G. Anderman and L.R. Brantley, J. Phys. Chem. Solids, 33 (1972) 467.
[40]　J.E. Eldridge and E.D. Palik, in Ref. [11], p. 775.
[41]　J.E. Eldridge and P.R. Staal, Phys. Rev. B, 16 (1977) 4608.
[42]　I. Ohlidal and K. Navratil, in Ref. [12], p. 1021.
[43]　H. Harting, Stzungsber. Deutsch. Akad. Wiss. Ber., 4 (1948) 1.
[44]　K.F. Pai, T.J. Parker, N.E. Tornberg, R.P. Lowndes and W.G. Chambers, Infrared Physics, 18 (1978) 199.
[45]　D.F. Edwards and H.R. Philipp, in Ref. [11], p. 665.
[46]　F. Peter, Z. Phys., 15, (1923) 358.
[47]　D.F. Edwards and E. Ochoa, J. Opt. Soc. Am., 71 (1981) 607.
[48]　G. Guizzetti and A. Borghesi, in Ref. [11], p. 525.
[49]　J.N. Zemel, J.D. Jensen and R.B. Schoolar, Phys. Rev. A, 140 (1965) 330.
[50]　R. Geick, Phys. Lett., 10 (1964) 51.
[51]　S.A. Alterovitz and J.A. Woollam, in Ref. [12], p. 705.
[52]　W.J. Choyke and L. Patrick, J. Opt. Soc. Am., 58 (1968) 377.
[53]　(a) W.G. Spitzer, D.A. Kleinman and C.J. Frosch, Phys. Rev., 113 (1959) 133. (b) W.G. Spitzer, D.A. Kleinman, C.J. Frosch and D.J. Walsh, in: J.R. O'Connor and J. Smiltens (eds.), Silicon Carbide, A High Temperature Semiconductor. Pergamon, New York, 1960, pp. 347.
[54]　F. Gervais, in Ref. [12], p. 1035.
[55]　M. Cardona, Phys. Rev., 140 (1965) A651.
[56]　W.G. Spitzer, R.C. Miller, D.A. Kleinman and L.E. Howarth, Phys. Rev., 126 (1962) 1710.
[57]　E.D. Palik and A. Addamiano, in Ref. [11], p. 597.
[58]　A.N. Pikhtin and A.D. Yaskov, Sov. Phys. Semicond., 12 (1978) 622.
[59]　T. Deutsch, Proc. Int. Conf. Phys. Semicond., 6th Exeter, The Institute of Physics and the Physical Society, London, 1962, pp. 505.
[60]　L. Ward, in Ref. [12], p. 579.
[61]　A.B. Francis and A.J. Carlsson, J. Opt. Soc. A., 50 (1960) 118.
[62]　A. Manabe, A. Mitsuishi and H. Yoshinga, Jpn. J. Appl. Phys., 6 (1967) 593.
[63]　T.M. Cotter, M.E. Thomas and W.J. Troph, in Ref. [12], p. 899.
[64]　M.J. Dodge, Appl. Opt., 23 (1984) 1980.
[65]　A.S. Barker, Phys. Rev., 136 (1964) A1290.
[66]　V.C. Farmer, in: V.C. Farmer (ed.), The Infrared Spectra of Minerals. Mineralogical Society of London, UK, 1974, pp. 183.
[67]　T.M. Bienewski and S.J. Czyzak, J. Opt. Soc. Am., 53 (1963) 496.
[68]　R. Buscall, Colloids Surf. A, 75 (1993) 269.
[69]　C. Wong, Y.Y. Teng, J. Ashok and P.L.H. Varaprasad, in Ref. [12], p. 789.

[70] S.H. Wemple, M. Didomenico, Jr. and I. Camlibel, J. Phys. Chem. Solids, 29 (1968) 1797.

[71] D.F. Edwards and R.H. White, in Ref. [12], p. 805.

[72] H.W. Newkirk, D. K. Smith, and J. S. Kahn, Am. Mineral., 51 (1966) 141.

[73] E. Loh, Phys. Rev., 166 (1968) 673.

[74] G. Busca, G. Ramis, J.M. Gallardo Amores, V.S. Escribano and P. Piaggio, J. Chem. Soc. Faraday Trans., 90 (1994) 3181.

[75] P.M. Claesson, Forces between surfaces immersed in aqueous solutions. Thesis, Royal Institute of Technology, Stockholm, Sweden, 1986.

[76] A.L. Weisenhorn, P.K. Hansma, T.R. Albrecht and C.F. Quate, Appl. Phys. Lett., 54 (1989) 2651.

[77] U. Hartmann, Adv. Mater., 2 (1990) 594.

[78] J.L. Hutter and J. Bechhoefer, J. Vac. Sci. Technol. B, 12 (1994) 2251.

[79] J.L. Hutter and J. Bechhoefer, J. Appl. Phys., 73 (1993) 4123.

[80] X.-Y. Lin, F. Creuzet and H. Arribart, J. Phys. Chem., 97 (1993) 7272.

[81] T.J. Senden, C.J. Drummond and P. Kekicheff, Langmuir, 10 (1994) 358.

[82] W.A. Ducker, T.J. Senden and R.M. Pashley, Nature, 353 (1991) 239.

[83] I. Larson, C.J. Drummond, D.Y.C. Chan and F. Grieser, J. Am. Chem. Soc., 115 (1993) 11885.

[84] S. Biggs and P. Mulvaney, J. Chem. Phys., 100 (1994) 8501.

[85] S. Biggs and T.W. Healy, J. Chem. Soc. Faraday Trans., 90 (1994) 3415.

[86] A. Milling, P. Mulvaney and I. Larson, J. Colloid Interface Sci., 180 (1996) 460.

[87] A. Meurk, P. Luckham and L. Bergström, Langmuir, submitted.

[88] H.D. Ackler, R.H. French and Y.-M. Chiang, J. Colloid Interface Sci., 179 (1996) 460.